Available online at www.sciencedirect.com
SCIENCE DIRECT®
Coordination Chemistry Reviews 248 (2004) 185–203
COORDINATION CHEMISTRY REVIEWS
www.elsevier.com/locate/ccr

Review

Hydrogen bonding of 18-crown-6 ether to ruthenium–ammine complexes at second sphere

Isao Ando*

Department of Chemistry, Faculty of Science, Fukuoka University, Nanakuma 8-19-1, Jonan-ku, Fukuoka 814-0180, Japan

Received 24 June 2002; accepted 31 October 2003

Dedicated to Professor H. Kurihara on the occasion of his 70th birthday

Contents

Abstract 185
1. Introduction 185
2. Adduct formation of mononuclear ruthenium complexes with 18-crown-6 ether through hydrogen bonding 186
3. Modification of electrochemical properties of ruthenium complexes caused by formation of hydrogen bonds 194
4. Stability constants of crown ether adducts 198
5. Adduct formation of mixed-valence binuclear complex 200
6. Conclusions 202
References 202

Abstract

The interaction with the second sphere of the complexes has been studied for a series of ruthenium–ammine complexes with 18-crown-6 (18C6) ether. Spectroscopic studies (UV, IR and NMR) gave the information about the nature of interaction and the interaction sites. Mononuclear ruthenium–ammine complexes form adducts through hydrogen bonding between the ammines coordinating to ruthenium and the ether oxygens of crown ethers. The position of the ammines interacting with the crown ether and the stoichiometry vary depending on the valence of central metal. The adduct formation perturbed the electronic state of the central metal ion and causes a modification of the properties of the complexes. The adduct formation through hydrogen bonding has been investigated focusing on the electrochemical properties of the complexes. Hydrogen bonding in the second sphere of the complex gave a prominent modification of electrochemical properties of the ruthenium–ammine complexes. Several factors were elucidated to influence on the modification of the electrochemical properties. The adduct formation with 18-crown-6 ether was also examined for a delocalized mixed-valence binuclear complex. The adduct formation stabilized the mixed-valence state of Ru(II)–Ru(III) and thereby the delocalized valence was trapped on each ruthenium atom. This was demonstrated by the isolation of the adducts.

Keywords: Ruthenium–ammine complexes; Crown ethers; Hydrogen bonding

1. Introduction

Recently, non-covalent bonds have been recognized to be important in biological processes such as substrate binding to a receptor protein, enzymatic reactions, assembling of protein–protein complexes, immunological antigen–antibody association, intermolecular reading, etc. [1]. For transition metal complexes, the coordinating influence extends beyond their covalently–bonded first-sphere ligands to non-covalently bound chemical species in the second sphere [2,3].

Ligands in the first coordination sphere of a transition metal complex can interact non-covalently with neutral molecules or charged species to give a second-sphere or outer-sphere complex. The idea of second-sphere coordination was first advanced by Werner [4]. On the basis of second-sphere coordination, he explained a number of phenomena, which included the formation of addition compounds between amines and coordinatively-saturated

* Tel.: +81-92-871-6631; fax: +81-92-865-6030.
E-mail address: isaoando@fukuoka-u.ac.jp (I. Ando).

0010-8545/$ – see front matter © 2003 Elsevier B.V. All rights reserved.
doi:10.1016/j.cct.2003.10.011

Table 1
Spectral and redox data for $[Ru(NH_3)_5(4\text{-CN-Mepy})](PF_6)_3$[a] in various solvents[b]

Solvent	λ_{max}[c] (nm)	$E_{1/2}$ (V) vs. SCE
Nitromethane	529	0.83
Nitrobenzene	545	
Benzonitrile	558	
Acetonitrile	543	0.77
Propylene carbonate	546	0.69
Cyclopentanone	562	
Acetone	550	0.76
N-Methylformamide	577	0.47
Tri-*n*-butyl phosphate	579	
Dimethylformamide	581	0.50
Dimethylacetamide	586	
Dimethyl sulfoxide	584	0.47
Hexamethylphosphoramide	619	

[a] 4-CN-Mepy: 4-cyano-*N*-methylpyridinium.
[b] Taken from [5].
[c] Band maxima of MLCT transitions.

Table 2
Abbreviations for the ligands used in this study

Ligand	Abbreviation
Pyridine	py
4-Aminopyridine	ampy
4-(Dimethylamino)pyridine	dmapy
Isonicotinamido	isn
2,2′-Bipyridine	bpy
4,4′-Bipyridine	4,4′-bpy
4,4′-Dimethyl-2,2′-bipyridine	Me_2-bpy
5-Nitro-1,10-phenanthroline	NO_2-phen
2,2′,2″-Terpyridine	trpy
4-(Dimethylamino)benzonitrile	dmabn
Pyrazine	pz
N-Methylpyrazinium	Mepz
N-Methylimidazole	MeIm
Dinitrogen	N2

trisacetylacetonato complexes, the role of solvents (e.g. H_2O) in the crystallization of complexes, and the observation that the molar optical rotations of chiral complexes depend strongly on the nature of solvents and the counterion. However, the nature of the forces involved in solvation was not well-understood at all at that stage. Since Werner made the proposal, developments in optical, spectroscopic, crystallographic, and theoretical techniques have revealed a wide range of other phenomena which can be accounted for on the basis of second-sphere coordination either in the solid state or in solution, or indeed both. The forces responsible for the second-sphere coordination include the whole range of non-covalent interaction, i.e. hydrogen bonding, polar and dipolar attractions, dispersion forces, and charge-transfer interactions.

Solvatochromism is shown in ruthenium–ammine complexes with the different number of ammine ligand which contain pyridine, polypyridine or pyridinium ligand [5–7]. Their ruthenium(II) complexes show the metal to ligand charge-transfer (MLCT) band (transition from the filled t_{2g} orbital of ruthenium(II) to the pyridine ligand LUMO) in the visible region. Their ruthenium(III) complexes also show the ligand to metal charge-transfer (LMCT) band (transition from the pyridine ligand HOMO to the unfilled t_{2g} orbital of ruthenium(III)) in visible region. Their energy was linearly dependent on the Gutmann's donor number (DN) [8] of a solvent and is responsible for solvatochromism. Table 1 summarizes the spectroscopic characteristics and the redox properties in various solvents for $[Ru(NH_3)_5(4\text{-CN-Mepy})](PF_6)_3$ (4-CN-Mepy: 4-cyano-*N*-methylpyridinium) as an example [5].

The absorption maxima of the MLCT band of the complex in Table 1 varied from 529 nm in nitromethane to 619 nm in hexamethylphosphoramide and the redox potential also varied about 0.4 V depending on solvent. For the ruthenium–ammine complexes, solvents sometimes gave much greater modification in properties of complexes relative to that by displacement of a ligand in the first coordination-sphere by an other ligand. In solution, the complex is surrounded by solvent molecules and the properties of the complex are affected by the nature and the strength of the interaction of the ligands with the solvent in the second sphere. If an appropriate organic substrate would be chosen instead of a solvent, the substrate may preferentially interact only with a specific ligand in the first coordination sphere of the complex. In this case, an optimal combination of a complex with a substrate leads to a selective or specific second-sphere coordination, and be followed by new properties of the complex.

Crown ethers are capable of hydrogen bonding with protic ligands such as NH_3, H_2O, CH_3CN, etc. in the first coordination sphere of a complex [9–16]. Being inert and having a variety of redox potentials, ruthenium complexes are very suitable for detailed studies of redox properties of the complex caused by second-sphere coordination. This review focuses on the modification of redox properties of some ruthenium complexes caused by 18-crown-6 (18C6) ether and involving ammines as a protic ligand. Quantitative effects caused by second-sphere ligands on oxygen ligator atoms in oxidic solids have been reviewed [17]. Table 2 and Scheme 1 show the abbreviations of the ligands in ruthenium complexes and crown ethers used in this review.

2. Adduct formation of mononuclear ruthenium complexes with 18-crown-6 ether through hydrogen bonding

Ruthenium–ammine complexes show a charge-transfer band in the visible region sensitive to second-sphere coordination [5,6,18–24]. Ruthenium(II)–ammine complexes exhibit a MLCT (transition from ruthenium t_{2g} orbital to an aromatic ligand such as a pyridine derivative LUMO) band in the visible region and a π–π^* band of the aro-

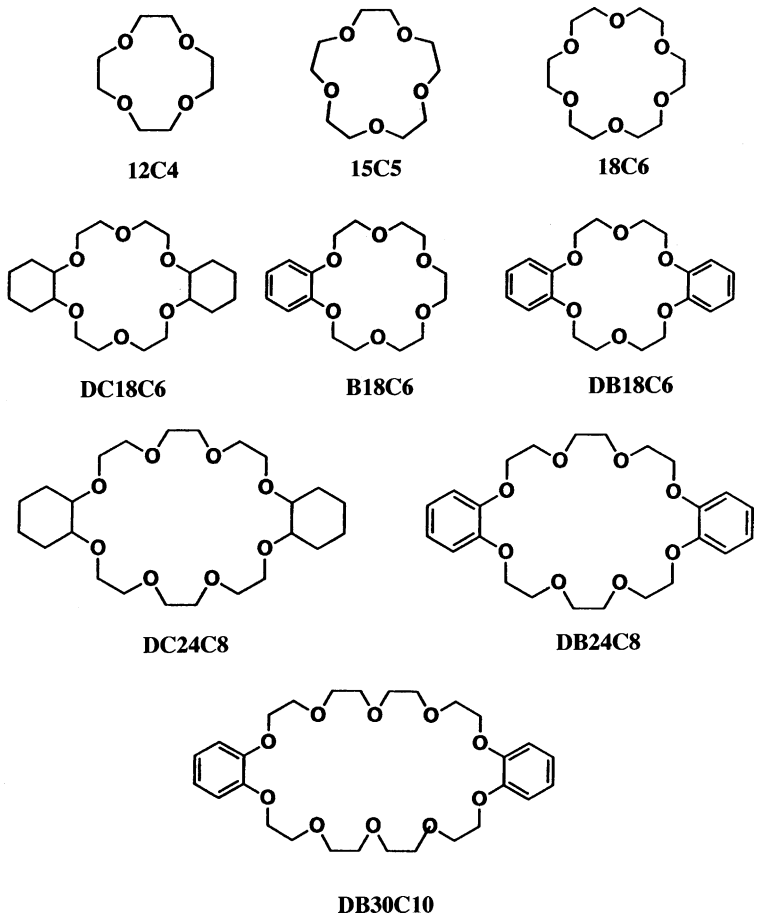

Scheme 1. Schematic representation and abbreviations of crown ethers used in this study.

matic ligand in the ultraviolet region [5,6,18–20,24]. On the other hand, ruthenium(III)–ammine complexes exhibit a LMCT (transition from the aromatic ligand HOMO to the unfilled t_{2g} orbital of ruthenium(III)) band in the visible region and a π–π^* band of the aromatic ligand in the ultraviolet region [21–23]. Adduct formation was spectrophotometrically investigated for ruthenium–ammine complexes and 18C6 systems [25–29]. Fig. 1 shows typical spectroscopic changes on addition of 18C6 to the ruthenium(II)– and ruthenium(III)–ammine complexes in acetonitrile. $[Ru(NH_3)_5(4,4\text{-bpy})](PF_6)_2$ showed a MLCT band at 474 nm, [20] and *trans*-$[Ru(NH_3)_4(dmapy)_2](PF_6)_3$ showed a CT band at 636 nm which was ascribed to a LMCT band similar to $[Ru(NH_3)_5(dmapy)](PF_6)_3$ [22,23]. The MLCT band of the ruthenium(II)–ammine complex shifted toward longer wavelength with increasing 18C6 concentration. On the contrary, the LMCT band of the ruthenium(III)–ammine complex showed a blue shift by adding 18C6. These spectroscopic changes may be attributed to the second-sphere coordination of 18C6 to the ruthenium complex through hydrogen bonding between the ammines coordinating to ruthenium and the ether oxygens of 18C6, as demonstrated for other ammine/crown ether adducts by single crystal X-ray method [13,15,30–33].

Spectroscopic features observed above can be rationalized as follows [25]. Both ruthenium(II)– and ruthenium(III)–ammine complexes are stabilized by formation of hydrogen bonds between the ammines coordinating to ruthenium and the ether oxygens of 18C6. The ammine–18C6 interaction is expected to be stronger in the ruthenium(III) than in the ruthenium(II) complex because the ammine proton becomes more acidic when coordinated to a higher valent metal ion. Thus, in the 18C6 adduct of the ruthenium(II)–ammine complex, the charge-transfer state is more stabilized relative to the ground state, because the polarization of nitrogen–hydrogen bond of the coordinated ammine increases with a transfer of electron from ruthenium to an ancillary ligand. Accordingly, hydrogen bonding with 18C6 causes a red shift of the MLCT band of ruthenium(II)–ammine complex. Similarly, for the ruthenium(III)–ammine complex, the ground state is more stabilized relative to the charge-transfer state in its 18C6 adduct, and the ruthenium(III)–ammine complex exhibits a blue shift of the LMCT band.(Scheme 2).

Other ruthenium–ammine complexes exhibited similar spectroscopic changes to those mentioned above on addition of 18C6, though the complexes contain different numbers of ammine ligands [28]. This suggests that such complexes

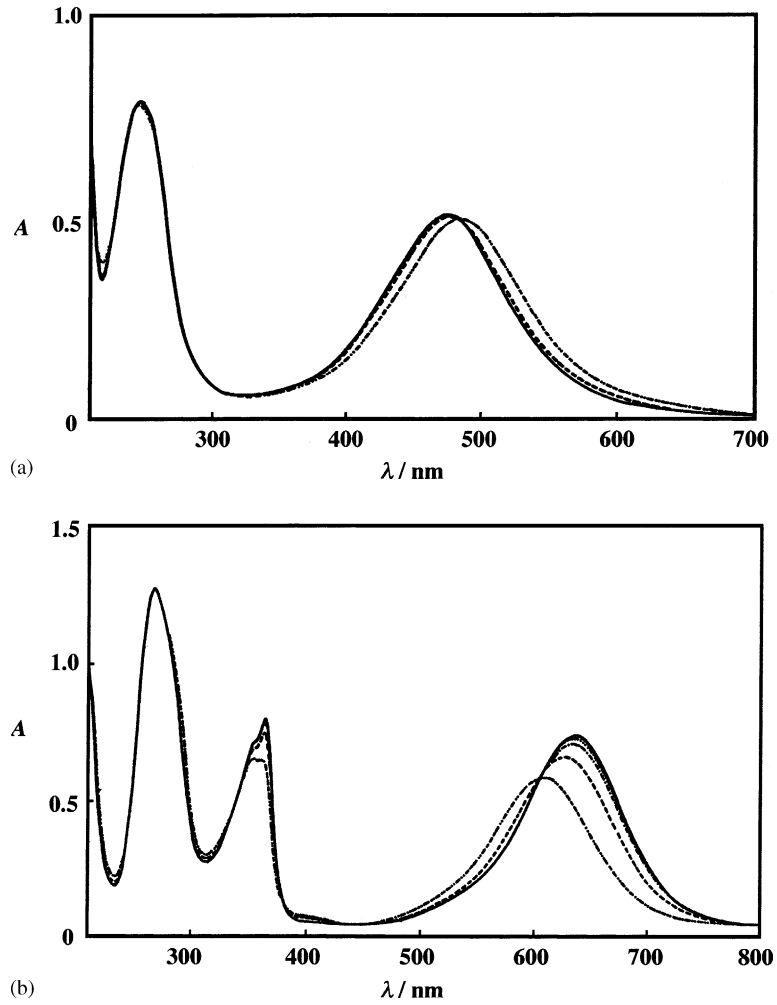

Fig. 1. Spectral changes of ruthenium–ammine complexes on addition of 18C6 in acetonitrile for (a) $[Ru(NH_3)_5(4,4'\text{-bpy})](PF_6)_2$ and (b) *trans*-$[Ru(NH_3)_4(dmapy)_2](PF_6)_3$. [complex] = 5.00×10^{-5} mol dm^{-3}; [18C6]/[complex] = 0 (—), 1 (···), 10 (-·-·-), 100 (- - -), and 1000 (-···-).

with different aromatic ligands form an adduct with 18C6 through hydrogen bonding between the ammines coordinating to ruthenium and the ether oxygens of 18C6. The shifts of the CT bands offer information about the equilibria of adduct formation with 18C6 [34]. Unfortunately, the equilibrium constants could not be evaluated owing to the small magnitude of their shifts. However, the magnitude of the shift can be considered as a tentative measure of the stability of their adduct. Table 3 summarizes the magnitude of the shift of their CT bands, $\Delta\tilde{\nu}_{max}$, in cm^{-1} units on

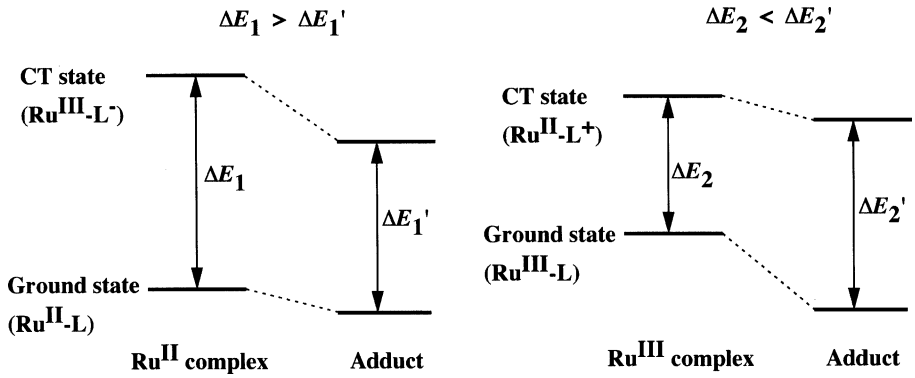

Scheme 2. Schematic energy level diagrams of the ground state and the charge-transfer state for ruthenium(II) and ruthenium(III) complexes and their adducts.

Table 3
Values of λ_{max} of MLCT or LMCT bands for ruthenium–ammine complexes and $\Delta\tilde{\nu}_{max}$ on addition of a 100-fold excess of 18C6 in acetonitrile

Complex	L, L′	λ_{max} (nm)	$\Delta\tilde{\nu}_{max}$ ($10^3\,cm^{-1}$)
$[Ru(NH_3)_5(L)](PF_6)_3$	dmapy	595 (16.81)	0.76
	ampy	514 (19.46)	0.62
	Mepz	540 (18.52)	0
$[Ru(NH_3)_5(L)](PF_6)_2$	py	408 (24.51)	−0.18
	4,4′-bpy	474 (21.10)	−0.14
	isn	468 (21.37)	−0.18
	pz	458 (21.83)	−0.09
cis-$[Ru(NH_3)_4(L)](PF_6)_2$	Me_2-bpy	524 (19.08)	−0.33
	bpy	524 (19.08)	−0.32
	NO_2-phen	515 (19.42)	−0.41
cis-$[Ru(NH_3)_4(L)_2](PF_6)_3$	dmapy	620 (16.13)	0.56
	ampy	534(18.73)	0.69
cis-$[Ru(NH_3)_4(L)_2](PF_6)_2$	py	409 (24.45)	−0.18
	isn	469 (21.32)	−0.09
trans-$[Ru(NH_3)_4(L)_2](PF_6)_3$	dmapy	636 (15.72)	0.20
	ampy	538 (18.59)	0.10
trans-$[Ru(NH_3)_4(L)_2](PF_6)_2$	py	423 (23.64)	−0.06
	isn	482 (20.75)	−0.09
mer-$[Ru(NH_3)_3(L)](PF_6)_2$	trpy	541 (18.48)	−0.43
cis-$[Ru(NH_3)_2(L)_2](PF_6)_2$	bpy	491 (20.37)	−0.13
$[Ru(NH_3)(L)(L')](PF_6)_2$	trpy, Me_2-bpy	462 (21.65)	0
	trpy, bpy	458 (21.83)	−0.04
$[Ru(L)_3](PF_6)_2$	bpy	452 (22.12)	0

The values in parentheses are $\tilde{\nu}_{max}$ in $10^3\,cm^{-1}$ units.

adding a 100-fold excess of 18C6. Any trends in $\Delta\tilde{\nu}_{max}$ are not clear for individual ruthenium complexes because of their small values. However, it is clear that the $|\Delta\tilde{\nu}_{max}|$ caused by the adduct formation is larger for ruthenium(III) complexes than for ruthenium(II) complexes in tetraammine and pentaammine complexes. This is understandable in terms of the stronger acidity of ammine ligands coordinating to the ruthenium(III) metal center and supports the rational interpretation for the spectroscopic change of the ruthenium complex upon addition of 18C6.

The magnitude of the shift of the CT bands is dependent on the solvent; the CT bands of the ruthenium–ammine complexes showed no shift caused by the addition of 18C6 in polar solvent such as DMF, DMSO, and H_2O. In order to obtain information about the interaction of the ammine ligands with the ether oxygen, the shift, $\Delta\tilde{\nu}_{max}$, in the presence of 18C6 in 100-fold excess was examined in various solvents [26]. Attempts failed to correlate $\Delta\tilde{\nu}_{max}$ with parameters such as the donor number, the acceptor number, Reichart's E_T-value and Kosower's Z-value of the solvents. However, $\Delta\tilde{\nu}_{max}$ gave linear correlations with the reciprocal dielectric constant of the solvents as shown in Fig. 2, although the alkylnitriles show different relationships from the other solvents examined. $\Delta\tilde{\nu}_{max}$ increases with decreasing dielectric constants of the solvents, indicating that the interaction between the complex and 18C6 becomes stronger as the electrostatic field of the medium becomes weaker. This fact makes the interpretation of the spectroscopic change induced by the adduct formation more evident; that is, the ruthenium–ammine complexes interact with 18C6 through hydrogen bonding. The difference between the alkylnitrile and the other solvents is presumably attributable to dissimilar modes of solvation.

Crown ethers other than 18C6 induced similar changes in the spectra of ruthenium–ammine complexes, but with a smaller magnitude than did 18C6 [27]. The adduct formation appears to be influenced by the flexibility of the crown ring (see in Section 3).

The stoichiometry for adduct formation was examined by the Job's continuous variation method, taking advantage of the change in absorbance of the CT bands on addition of 18C6 [26,29]. The absorbance increments of the complex solution in the presence of 18C6, ΔA, were plotted against the mole fractions of the complex in the sum of the complex and 18C6 molecules. The plots in Fig. 3 clearly indicate that the ruthenium(II) complex forms an 1:1 adduct by interaction with one molecule of 18C6 but the ruthenium (III) complex further interacts with another molecule of 18C6, forming an 1:2 adduct. Table 4 summarizes the stoichiometries of adduct formation of ruthenium–ammine complexes with 18C6. The stoichiometry of adduct formation is independent of the number of ammine ligands and solvents. For the pentaammine complexes, the stoichiometry is dependent on the valence of the metal center. Thus,

Table 4
Stoichiometries of Adduct formation

Complex	Ratio of complex to 18C6			
	Acetonitrile	Propionitrile	Butyronitrile	2-Butanone
$[Ru(NH_3)_5(pz)](PF_6)_2$	1:1	1:1	1:1	1:1
$[Ru(NH_3)_5(isn)](PF_6)_2$		1:1		
$[Ru(NH_3)_4(bpy)](PF_6)_2$		1:1		
$[Ru(NH_3)_2(bpy)_2](PF_6)_2$		1:1		
$[Ru(NH_3)_5(dmapy)](PF_6)_3$	1:2		1:2	
$[Ru(NH_3)_5(ampy)](PF_6)_3$	1:2		1:2	

the composition of an adduct changes when the metal center is oxidized or reduced. However, it is sterically difficult for ruthenium(III)–ammine complexes with fewer ammine ligands to interact with more 18C6 molecules than one, specially for mono- and diammine complexes.

In order to determine the positions of interaction sites, the adduct formation of ruthenium complexes with 18C6 was investigated for representative ruthenium(II)– and ruthenium(III)–pentaammine complexes, $[Ru(NH_3)_5(pz)](PF_6)_2$ and $[Ru(NH_3)_5(dmapy)](PF_6)_3$, by ^1H NMR spectroscopy. Fig. 4 shows the ^1H NMR spectrum of $[Ru(NH_3)_5(pz)](PF_6)_2$ in deuterated acetone [35]. Signals of ammine protons were separately observed at 2.65 and 3.48 ppm and attributed to the protons of *cis*- and *trans*-ammines coordinating to ruthenium(II), respectively;[36,37] those of the aromatic protons were observed at 8.22 and 8.96 ppm. The chemical shifts of their signals were examined at various 18C6 concentrations and the results are shown in Fig. 5. The chemical shift of the *trans*-ammine proton changed toward a lower magnetic field with increasing 18C6 concentration. This downfield shift of the *trans*-ammine proton signal indicates that the adduct is formed through hydrogen bonding between the *trans*-ammine proton of the ruthenium(II) complex and the ether oxygen of 18C6. On the other hand, the signal of the *cis*-ammine proton shifted slightly to a higher magnetic field with increasing 18C6 concentration. This small upfield shift is presumably due to the partial desolvation around the *cis*-ammines caused by the formation of a hydrogen bond between the *trans*-ammine and 18C6. The change in chemical shifts of the aromatic protons caused by the addition of 18C6 reflects the perturbation of the π-electron density in the aromatic ring, because the increase in electron density on ruthenium caused by the adduct formation affects the degree of π-back donation of ruthenium(II) to the aromatic ligand as mentioned in the next section. These observations coincide with the stoichiometry of the adduct formation and indicate that the ruthenium(II) complexes form an 1:1 adduct with 18C6 through hydrogen bonding between the *trans*-ammine of the complex and the ether oxygen of 18C6, as schematically depicted in Scheme 3.

For the ruthenium(III)–pentaammine complex, $[Ru(NH_3)_5(dmapy)](PF_6)_3$, the signals of the ammine protons were observed at an extremely low magnetic field and were broad and weak due to the paramagnetic effect of the ruthenium(III) center. The signals at 117 and 157 ppm are attributed to the *cis*- and *trans*-ammine protons, respectively, by their integral ratio. Both signals shifted toward a lower magnetic field on adding 18C6 as shown in Fig. 6. The downfield shift of the *cis*-ammine signal is much greater than that of the *trans*-ammine signal. This indicates that 18C6 forms stronger hydrogen bonds with the *cis*-ammine and simultaneously weaker ones with the *trans*-ammine of the complex. Therefore, taking the stoichiometry of adduct

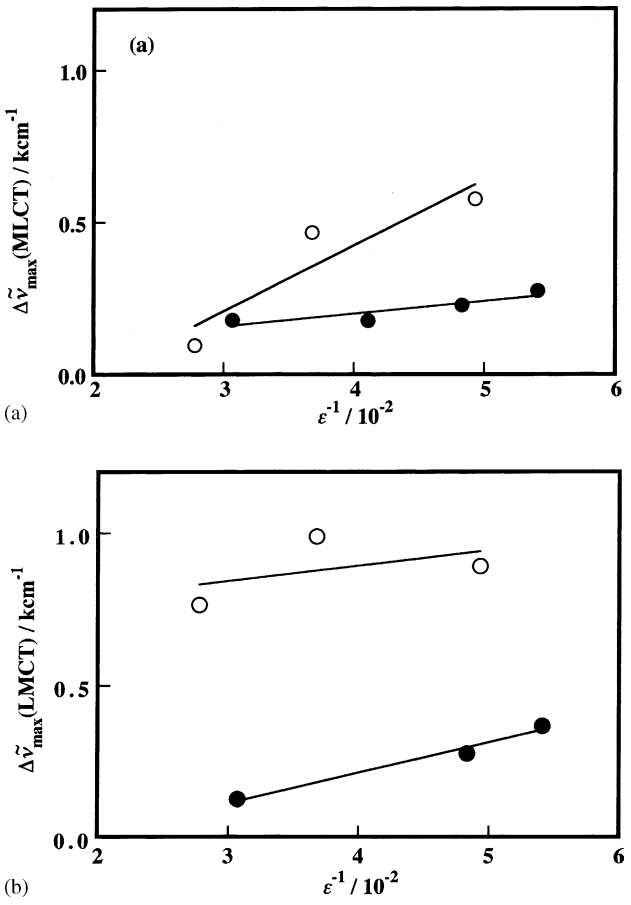

Fig. 2. Correlation between $\Delta\tilde{\nu}_{max}$ (CT) and the reciprocal dielectric constants of the solvents: (a) $[Ru(NH_3)_5(pz)](PF_6)_2$ and (b) $[Ru(NH_3)_5(dmapy)](PF_6)_3$. The open circles represent the data in alkylnitriles and the filled circles are the data in alcohols and ketone.

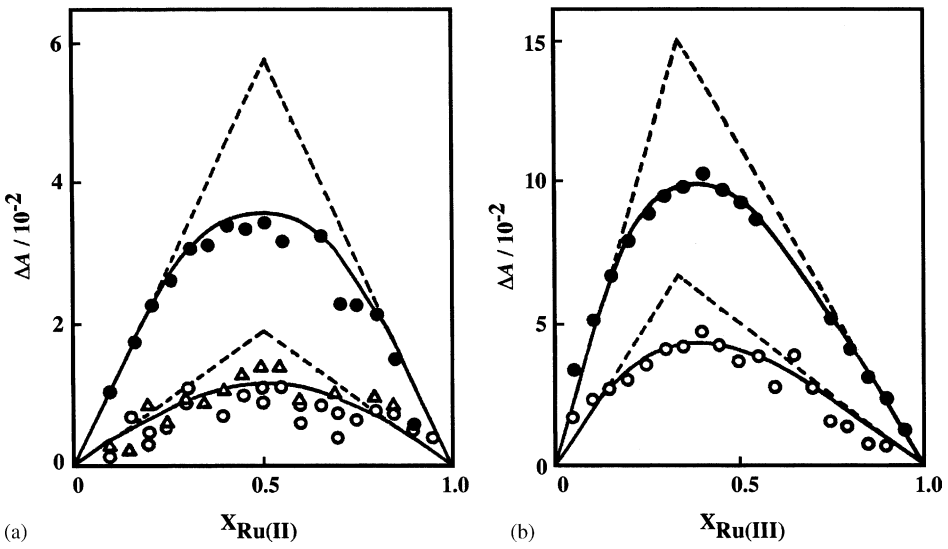

Fig. 3. Plots of the absorbance increments of the complex solutions in the presence of 18C6, ΔA, against the mole fractions of the complex for (a) $[Ru(NH_3)_5(pz)](PF_6)_2$ in acetonitrile (○), propionitrile (●) and 2-butanone (△); (b) $[Ru(NH_3)_5(dmapy)](PF_6)_3$ in acetonitrile (○) and butyronitrile (●).

formation for the ruthenium(III) complex into consideration, we conclude that the 1:2 adduct is formed primarily through hydrogen bonding between the *cis*-ammine of the ruthenium(III) complex and two molecules of 18C6, and supplementarily through hydrogen bonding between the *trans*-ammine and the 18C6 bonded to the *cis*-ammines, as schematically depicted in Scheme 3.

The position of the ammines interacting with 18C6 and the stoichiometry vary depending on the valence of the ruthenium center. This adduct formation is somewhat dissimilar to that of a large cyclic crown ether with tetraammineruthenium complex. Yoon et al. reported the crystal structure of the adduct dibenzo-42-crown-14-tetraammine(1,10-phenanthroline)ruthenium(II) bis(hexafluorophosphate)dichloromethane solvate [38]. As can be seen from Fig. 7, the ruthenium complex is located deep within the U-shaped cavity formed by folding of the flexible crown ether. This conformation allows all the ammine ligands of the complex to form multiple hydrogen bonds with the crown ether and brings about π-stacking between the aromatic rings of the ruthenium complex and the dibenzo-crown ether. However, 18C6 cannot form hydrogen bonds with the all ammine ligands of the pentaammine complex because of being a small

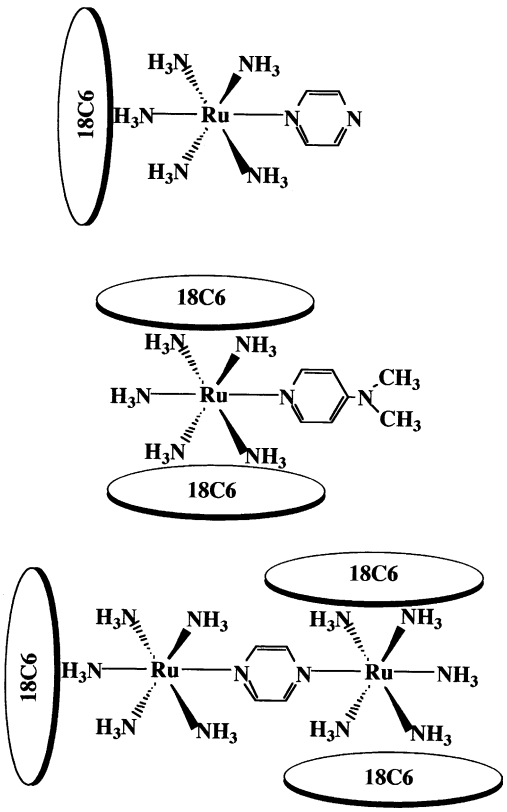

Scheme 3. Schematic representations of crown ether adducts for ruthenium(II)–ammine complex, ruthenium(III)–ammine complex, and mixed-valence binuclear ruthenium(II, III)–ammine complex.

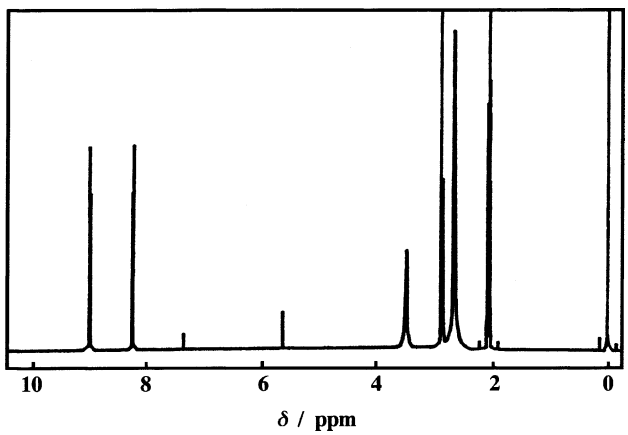

Fig. 4. ^1H NMR spectrum of $[Ru(NH_3)_5(pz)](PF_6)_2$ in deuterated acetone ([complex] = 1.0×10^{-2} mol dm^{-3}).

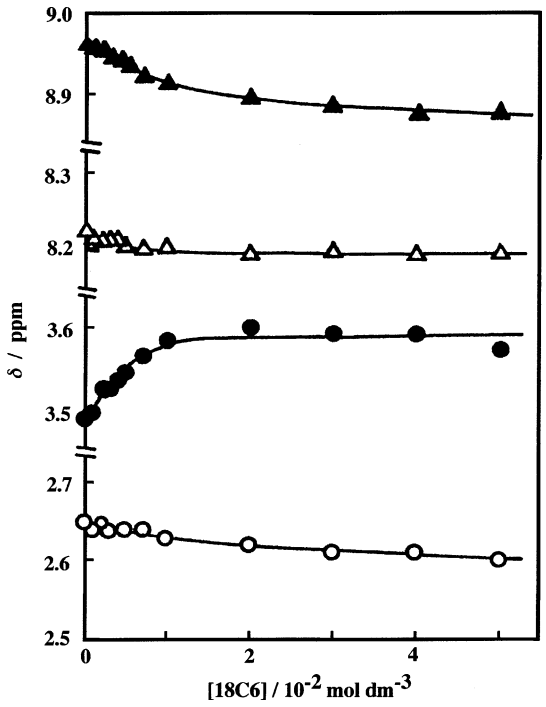

Fig. 5. Dependence of the chemical shifts of the 2,6-protons (△) and 3,5-protons (▲) of pyrazine and the *cis*-ammine (○) and *trans*-ammine protons (●) of $[Ru(NH_3)_5(pz)](PF_6)_2$ on 18C6 concentration ([complex] = 1.0×10^{-2} mol dm^{-3}).

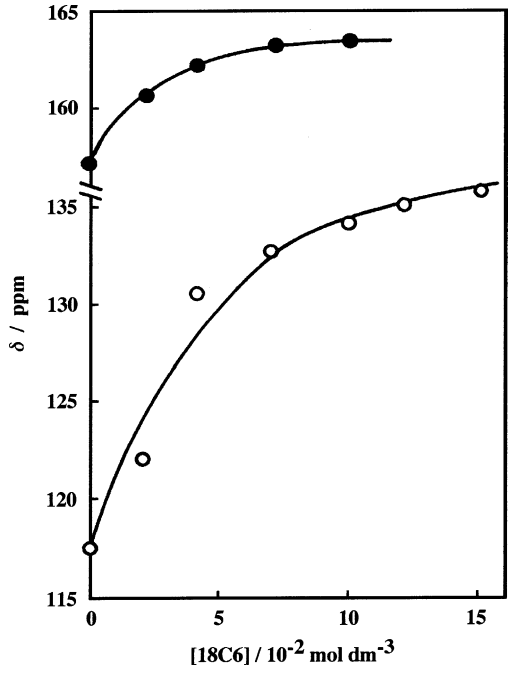

Fig. 6. Dependence of the chemical shifts of the *cis*-ammine (○) and *trans*-ammine protons (●) of $[Ru(NH_3)_5(dmapy)](PF_6)_3$ on 18C6 concentration ([complex] = 1.0×10^{-2} mol dm^{-3}).

cyclic ether in size. Thus, for the ruthenium-pentaammine complexes, 18C6 exhibits adduct formation with different stoichiometry depending on the valence of the ruthenium, i.e., depending on the acidity of ammine of the complex.

Further evidence on the stoichiometry was obtained by isolation of 18C6 adducts. 18C6 adducts were isolated for $[Ru(NH_3)_5(pz)](PF_6)_2$, $[Ru(NH_3)_5(dmapy)](PF_6)_3$, and $[(NH_3)_5Ru(pz)Ru(NH_3)_5](PF_6)_5$ as typical ruthenium(II)– and ruthenium(III)–ammine complexes, and a mixed-valence binuclear complex [39]. Adduct formation for a mixed-valence binuclear complex is described in Section 5.

The analytical data of the prepared adducts agreed with the composition in solution shown in Scheme 3 for the ruthenium(II) and the ruthenium(III) complexes. These results revealed that the ruthenium(II)–ammine complex forms an ordinary 1:1 (complex to 18C6) adduct with 18C6, whereas the ruthenium(III)–ammine complex forms an adduct with 18C6 with an unusual stoichiometry of 1:2. Furthermore, only the asymmetric 1:3 adduct with 18C6 was isolated for the mixed-valence binuclear complex among other adducts proposed in Scheme 5, although it is possible sterically for the binuclear complex to form 1:1 to 1:4 adducts with 18C6. This implies that the 1:3 adduct is the stable and predominant species in solution, with distinct $Ru(NH_3)_5^{2+}$ and $Ru(NH_3)_5^{3+}$ units in the complex. This is consistent with the electrochemical behavior of the mixed-valence binuclear complex on addition of 18C6 as described in Section 5.

The IR spectra of the complexes and their adducts were measured and the frequencies of N–H, C–H, and C–O–C stretching vibrations are listed in Table 5. The bands of the N–H stretching vibration broadened and shifted to lower frequency in every 18C6 adduct, indicating that the coordinating ammines form hydrogen bonds. Furthermore, the C–O–C stretching vibrations of all 18C6 adducts were observed at lower frequencies than that of free 18C6 [40] indicating that the ether oxygens of 18C6 participate in hydrogen bonding. A similar reduction in frequency of the C–O–C stretching vibration has been observed for the adduct of tin(IV) complexes with 18C6 involving hydrogen bonding between 18C6 and water molecules [16]. These results reveal that the adducts of ruthenium–ammine complexes with 18C6 involve hydrogen bonds between the coordinating ammines to ruthenium and ether oxygens of 18C6.

The reflectance spectra of the complexes and their adducts were measured in the solid state and were compared with the estimated spectra in 1,2-dichloroethane. Table 6 summarizes the $\tilde{\nu}_{max}$ values of MLCT and LMCT bands in solid state. The spectra of the ruthenium–ammine complexes in 1,2-dichloroethane could not be measured due to the insolubility of the complex. The spectra of the complexes in 1,2-dichloroethane were estimated as below, taking advantage of the well-known solvatochromism of ruthenium–ammine complexes [5,6]. The electronic spectra of $[Ru(NH_3)_5(pz)](PF_6)_2$ and $[Ru(NH_3)_5(dmapy)](PF_6)_3$ were measured in several solvents with different donor number (DN), and $\tilde{\nu}_{max}$ values of MLCT and LMCT bands

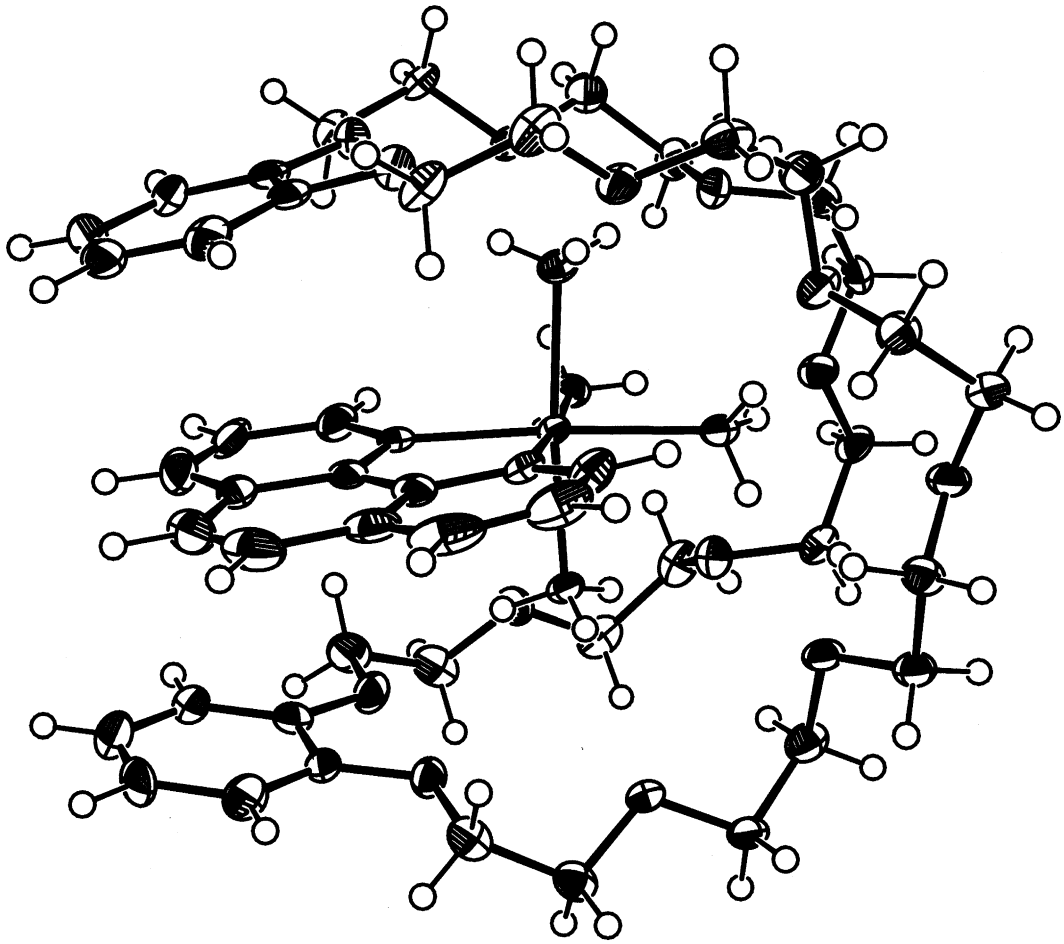

Fig. 7. ORTEP drawing of the $[Ru(NH_3)_4(phen)]^{2+}$–DB42C14 adduct reported in [38].

Table 5
IR spectra of ruthenium–ammine complexes and their 18-crown-6 ether adducts

	$\tilde{\nu}_{N-H}$ (cm^{-1})		$\tilde{\nu}_{C-H}$ (cm^{-1})	$\tilde{\nu}_{C-O-C}$ (cm^{-1})
$[Ru(NH_3)_5(pz)](PF_6)_2$	3350	3280		
$[Ru(NH_3)_5(pz)](PF_6)_2{\cdot}(18C6)$	3320	3215	2800	1100
$[Ru(NH_3)_5(dmapy)](PF_6)_3$	3340	3260		
$[Ru(NH_3)_5(dmapy)](PF_6)_3{\cdot}(18C6)_2$	3300	3220	2900	1100
$[(NH_3)_5Ru(pz)Ru(NH_3)_5](PF_6)_5$	3310	3250		
$[(NH_3)_5Ru(pz)Ru(NH_3)_5](PF_6)_5{\cdot}(18C6)_3$	3250	3180	2900	1100

Table 6
The $\tilde{\nu}_{max}$ values of MLCT or LMCT bands for ruthenium–ammine complexes and their 18-crown-6 ether adducts

	$\tilde{\nu}_{max}$ (10^3 cm^{-1})		$\Delta\tilde{\nu}_{max}$[a] (10^3 cm^{-1})	
	Solid[b]	Solution[c]	Solid	Solution
$[Ru(NH_3)_5(pz)](PF_6)_2$	23.2	22.6		
$[Ru(NH_3)_5(pz)](PF_6)_2{\cdot}(18C6)$	21.9	20.5	−1.3	−2.1
$[Ru(NH_3)_5(dmapy)](PF_6)_3$	16.2	15.0		
$[Ru(NH_3)_5(dmapy)](PF_6)_3{\cdot}(18C6)_2$	18.9	17.3	2.7	2.3
$[(NH_3)_5Ru(pz)Ru(NH_3)_5](PF_6)_5$	19.8	18.0		
$[(NH_3)_5Ru(pz)Ru(NH_3)_5](PF_6)_5{\cdot}(18C6)_3$	19.5	17.5	−0.3	−0.5

[a] $\Delta\tilde{\nu}_{max} = \tilde{\nu}_{max}(\text{adduct}) - \tilde{\nu}_{max}$ (complex).
[b] The values are obtained from reflectance spectra.
[c] The values are in 1,2-dichloroethane and are obtained as described in text.

for the complexes are plotted against the donor number of the solvents in Fig. 8. The plots in Fig. 8 gave straight lines and the $\tilde{\nu}_{max}$ of the MLCT or LMCT band in 1,12-dichloroethane was evaluated from the intercept at DN = 0 for each complex. These values are listed in Table 6 as the $\tilde{\nu}_{max}$ values of MLCT or LMCT bands for the complex in solution. On the other hand, electronic spectra of the adducts in solution were obtained as follows. The complex was extracted with a 1,2-dichloroethane containing a large excess of 18C6, and the spectra of the extracted solution, in which the complex can exist only as an adduct, were measured. The results are also listed in Table 6.

In the solid state, as can be seen in Table 6, the MLCT band of $[Ru(NH_3)_5(pz)](PF_6)_2$ showed a red shift in their 18C6 adduct and the LMCT band of $[Ru(NH_3)_5(dmapy)](PF_6)_3$ showed a blue shift in their 18C6 adduct. In $[(NH_3)_5Ru(pz)Ru(NH_3)_5](PF_6)_5$, which contains both $Ru(NH_3)_5^{2+}$ and $Ru(NH_3)_5^{3+}$ units but delocalized valence, the MLCT band of the binuclear complex showed a red shift in their 18C6 adduct. The spectra of three complexes in Table 6 and their 18C6 adducts in 1,2-dichloroethane exhibited a similar difference in wavenumber to the reflectance spectra mentioned above. The shifts of the CT band from the complex to the adduct are essentially identical both in the solid state and in solution for all complexes. These spectroscopic changes from the complex to the adduct are also consistent with those on adduct formation of ruthenium–ammine complexes with 18C6 in acetonitrile.

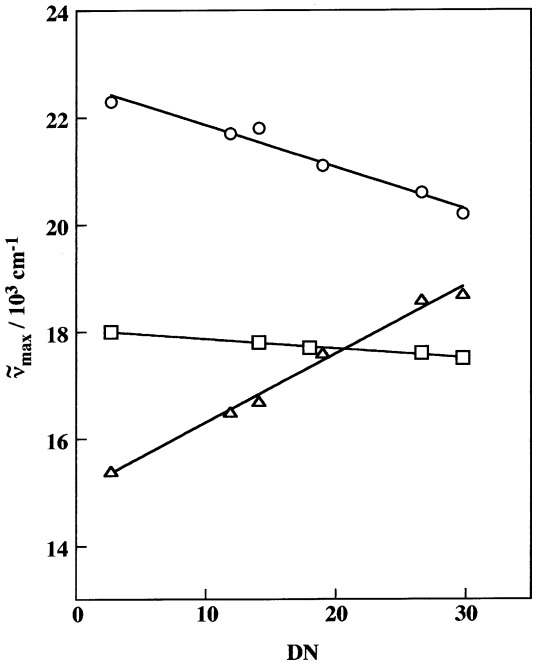

Fig. 8. Correlation between $\tilde{\nu}_{max}$ of the MLCT or LMCT band of the complex and the donor number of the solvent: $[Ru(NH_3)_5(pz)](PF_6)_2$ (○), $[Ru(NH_3)_5(dmapy)](PF_6)_3$ (△), and $[(NH_3)_5Ru(pz)Ru(NH_3)_5](PF_6)_5$ (□).

We conclude as schematically represented in Scheme 3 that a ruthenium–ammine complex forms an adduct with crown ethers through hydrogen bonding between the ammines coordinating to ruthenium and the ether oxygens of crown ethers; a ruthenium(II)–ammine complex forms a discrete 1:1 adduct by interacting with the *trans*-ammine of the complex, whereas a ruthenium(III)–ammine complex forms a 1:2 adduct with the crown ether by interacting with the *cis*-ammines of the complex.

3. Modification of electrochemical properties of ruthenium complexes caused by formation of hydrogen bonds

Hydrogen bonding with crown ethers should also affect the electrochemical behavior of the complexes. Therefore, changes in this behavior were examined with respect to adduct formation for a series of ruthenium–ammine complexes and crown ethers [28].

Adduct formation with a representative crown ether 18C6 was electrochemically investigated for the complexes in Table 7 in acetonitrile. Fig. 9 shows the typical change in the cyclic voltammogram by adding crown ethers to the complex. The cyclic voltammograms of all the complexes exhibited one redox couple in the range of −0.5 to +1.0 V versus ($AgNO_3$/Ag) which corresponds to the Ru(III)/Ru(II) redox process. The redox couple is symmetrical and shows a peak separation of about 60 mV for all complexes, [5,6,24,36,41–44]. When 18C6 was added to the solution of the complex, the redox couple shifted continuously toward a more negative potential with increasing 18C6 concentration, while maintaining its reversibility and without an appearance of any new processes. The dependence of $E_{1/2}$ on the 18C6 concentration was determined

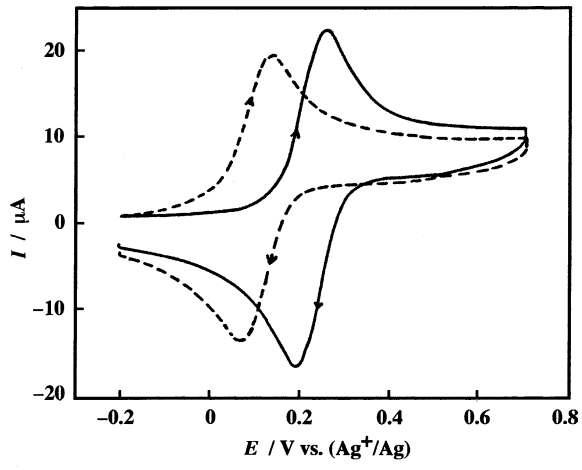

Fig. 9. Cyclic voltammograms of $[Ru(NH_3)_5(pz)](PF_6)_2$ in 0.10 mol dm^{-3} tetrabutylammonium hexafluorophosphate acetonitrile solution at a scan rate of 40 mV s^{-1}. Solid and dashed lines are the voltammograms in the absence and presence of 0.10 mol dm^{-3} 18C6, respectively ([complex] = 5.0×10^{-4} mol dm^{-3}).

Table 7
Limiting values of change in redox potential, $\Delta E_{1/2}$(lim), for Ru(III)–Ru(II) redox couples of ruthenium–ammine complexes caused by addition of 18C6 in acetonitrile[a]

Complex	L	$E_{1/2}$ (V) vs. (Ag^+/Ag)	$\Delta E_{1/2}$(lim) (mV)[b]
$[Ru(NH_3)_6](PF_6)_3$		−0.186 (3)	−169 (2)
$[Ru(NH_3)_5(L)](PF_6)_3$	Cl^-	−0.518 (2)	−162 (3)
	dmapy	−0.142 (3)	−121 (2)
	MeIm	−0.141 (2)	−128 (3)
	ampy	−0.127 (4)	−131 (2)
$[Ru(NH_3)_5(L)](PF_6)_2$	py	0.060 (4)	−129 (2)
	4,4′-bpy	0.096 (5)	−129 (3)
	isn	0.118 (5)	−133 (2)
	dmabn	0.146 (2)	−173 (2)
	pz	0.237 (3)	−131 (3)
	N_2[c]	0.830	−110
$[Ru(NH_3)_5(L)](PF_6)_3$	Mepz	0.661 (6)	−105 (2)
cis-$[Ru(NH_3)_4(L)](PF_6)_2$	Me_2-bpy	0.174 (4)	−124 (2)
	bpy	0.260 (3)	−122 (1)
	NO_2-phen	0.361 (4)	−111 (2)
cis-$[Ru(NH_3)_4(L)_2](PF_6)_3$	dmapy	−0.124 (2)	−96 (5)
	ampy	−0.077 (2)	−116 (4)
cis-$[Ru(NH_3)_4(L)_2](PF_6)_2$	py	0.280 (3)	−99 (7)
	isn	0.386 (5)	−120 (3)
trans-$[Ru(NH_3)_4(L)_2](PF_6)_3$	dmapy	−0.139 (4)	−68 (3)
	ampy	−0.112 (3)	−97 (12)
trans-$[Ru(NH_3)_4(L)_2](PF_6)_2$	py	0.253 (4)	−91 (6)
	isn	0.353 (2)	−124 (5)
mer-$[Ru(NH_3)_3(L)](PF_6)_2$	trpy	0.486 (3)	−70 (1)
cis-$[Ru(NH_3)_2(L)_2](PF_6)_2$	bpy	0.616 (4)	−57 (1)
$[Ru(NH_3)(L)(L')](PF_6)_2$	trpy, Me_2-bpy	0.730 (4)	−32 (9)
	trpy, bpy	0.786 (6)	−32 (1)
$[Ru(L)_3](PF_6)_2$	bpy	0.990	0

[a] The values in parentheses are the standard deviation in mV units. [complex] = 5.0×10^{-4} mol dm^{-3}.
[b] See text.
[c] The change in oxidation potential of the complex on adding of 200-fold excess of 18C6 to the complex solution.

in detail for the ruthenium complexes in Table 7. Fig. 10 shows typical examples of the dependence of the change in redox potential, $\Delta E_{1/2}$, on 18C6 concentration. Curve fittings of several type functions were applied to the dependences of $\Delta E_{1/2}$ on 18C6 concentration. The exponential function of Eq. (1) reproduced adequately the observed

$$\Delta E_{1/2} = \Delta E_{1/2}(\text{lim}) + A \exp(-B[18C6]) \quad (1)$$

dependences of $\Delta E_{1/2}$ for the complexes in Table 7. Thus, the limiting change in redox potential, $\Delta E_{1/2}$(lim), was evaluated from the dependences of $\Delta E_{1/2}$ on 18C6 concentration by the least square analysis of Eq. (1). The $\Delta E_{1/2}$(lim) values obtained are summarized in Table 7.

Fig. 11 shows the plot of $\Delta E_{1/2}$(lim) against the number of ammine ligands. In a roughly linear manner, $\Delta E_{1/2}$(lim) decreases with the number of ammine ligands; the relationship is linear for the complexes with ligands including only pyridine moieties in addition to the ammines. $\Delta E_{1/2}$(lim) is proportional to the difference between the stabilities of the ruthenium(II) and ruthenium(III) complexes due to adduct formation with 18C6. This shift is consistent with the greater acidity of ammine ligands coordinating to ruthenium(III) making the hydrogen bond stronger than that in the ruthenium(II) complex. In addition, the ruthenium(III)–ammine complex with fewer ammines can form hydrogen bonds with 18C6 to a lesser degree than the ruthenium(III)–pentaammine complex in its adduct. Therefore, the greater the number of ammine ligands, the greater the stabilization of ruthenium(III) complexes by adduct formation.

On the other hand, ligands other than ammines also contribute to $\Delta E_{1/2}$(lim). Because ligands such as pyridine behave as electron-accepting π-acids, the contribution of these ligands to $\Delta E_{1/2}$(lim) is opposite to that of the ammine; thus $\Delta E_{1/2}$(lim) becomes less negative with increasing pyridine moieties.

The plot in Fig. 11 shows that $\Delta E_{1/2}$(lim) is different for the complexes with the same number of ammine

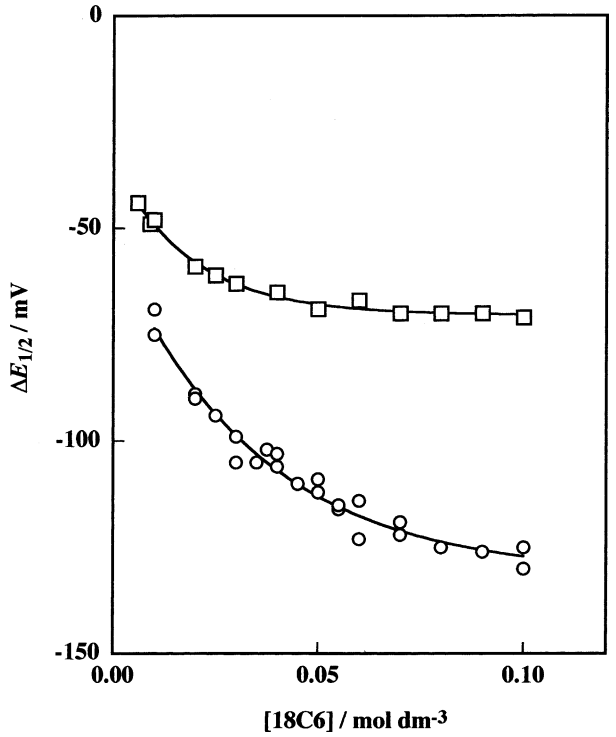

Fig. 10. Dependence of $\Delta E_{1/2}$ on 18C6 concentration for $[Ru(NH_3)_5(pz)](PF_6)_2$ (○) and $[Ru(NH_3)_3(trpy)](PF_6)_2$ (□). The values of $\Delta E_{1/2}$ were obtained from cyclic voltammograms measured at a scan rate of 40 mV s^{-1} in acetonitrile. Solid lines are the exponential regression lines of the data.

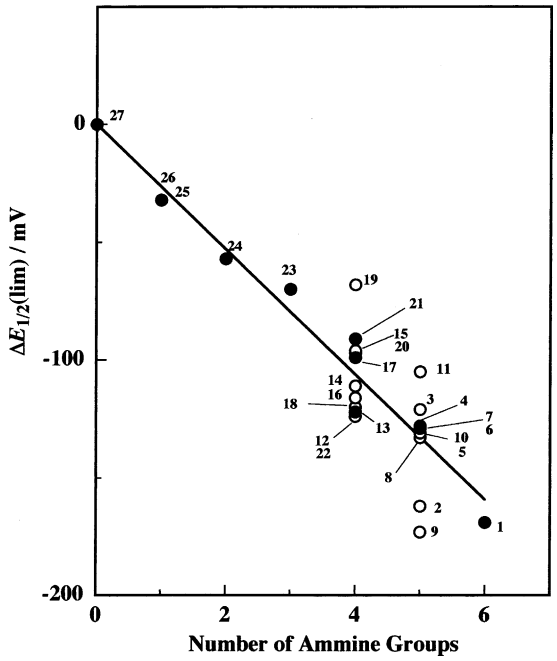

Fig. 11. Plot of the limiting change in redox potential caused by adduct formation, $\Delta E_{1/2}$(lim), against the number of coordinated ammines for the complexes in Table 7: (1) $[Ru(NH_3)_6](PF_6)_3$, (2) $[Ru(NH_3)_5(Cl)](PF_6)_2$, (3) $[Ru(NH_3)_5(dmapy)](PF_6)_3$, (4) $[Ru(NH_3)_5(MeIm)](PF_6)_3$, (5) $[Ru(NH_3)_5(ampy)](PF_6)_3$, (6) $[Ru(NH_3)_5(py)](PF_6)_2$, (7) $[Ru(NH_3)_5(4,4'\text{-bpy})](PF_6)_2$, (8) $[Ru(NH_3)_5(isn)](PF_6)_2$, (9) $[Ru(NH_3)_5(dmabn)](PF_6)_2$, (10) $[Ru(NH_3)_5(pz)](PF_6)_2$, (11) $[Ru(NH_3)_5(Mepz)](PF_6)_3$, (12) *cis*-$[Ru(NH_3)_4(Me_2\text{-bpy})](PF_6)_2$, (13) *cis*-$[Ru(NH_3)_4(bpy)](PF_6)_2$, (14) *cis*-$[Ru(NH_3)_4(NO_2\text{-phen})](PF_6)_2$, (15) *cis*-$[Ru(NH_3)_4(dmapy)_2](PF_6)_3$, (16) *cis*-$[Ru(NH_3)_4(ampy)_2](PF_6)_3$, (17) *cis*-$[Ru(NH_3)_4(py)_2](PF_6)_2$, (18) *cis*-$[Ru(NH_3)_4(isn)_2](PF_6)_2$, (19) *trans*-$[Ru(NH_3)_4(dmapy)_2](PF_6)_3$, (20) *trans*-$[Ru(NH_3)_4(ampy)_2](PF_6)_3$, (21) *trans*-$[Ru(NH_3)_4(py)_2](PF_6)_2$, (22) *trans*-$[Ru(NH_3)_4(isn)_2](PF_6)_2$, (23) *mer*-$[Ru(NH_3)_3(trpy)](PF_6)_2$, (24) *cis*-$[Ru(NH_3)_2(bpy)_2](PF_6)_2$, (25) $[Ru(NH_3)(trpy)(Me_2\text{-bpy})](PF_6)_2$, (26) $[Ru(NH_3)(trpy)(bpy)](PF_6)_2$, (27) $[Ru(bpy)_3](PF_6)_2$. Filled circles denote complexes with ligands including only the pyridine moiety in addition to the ammine ligands.

ligands: $\Delta E_{1/2}$(lim) varies from −105 to −173 mV and from −68 to −124 mV for pentaammine complexes and tetraammine complexes, respectively, and is hence dependent on the ancillary ligand, L. The dπ-electrons of the ruthenium-coordination center is distributed over the whole complex to some extent. By formation of a hydrogen bond of the coordinating ammine with 18C6, the electron density on the coordination center increases. However, the increased electron density is somewhat delocalized over the whole complex by redistribution through pπ–dπ back donation. Thus, a net increase in the electron density on the coordination center may be modified by the π-electron acceptability of L. Accordingly, $\Delta E_{1/2}$(lim), should be closely related to the π-electron acceptability of L acting as a π-acid.

The enthalpy change, ΔH_{sub}, for the substitution reaction of Eq. (2) is known to

$$[Ru(NH_3)_5(H_2O)]^{2+} + L \rightleftharpoons [Ru(NH_3)_5(L)]^{2+} + H_2O \quad (2)$$

correspond to the stabilization due to pπ–dπ back donation, because the difference in ΔH between the substitution reactions of $[Ru(NH_3)_5(H_2O)]^{2+}$ and $[Ni(H_2O)_6]^{2+}$ with L agreed with the stabilization energy caused by pπ–dπ back donation as estimated from spectroscopic investigation and, further, ΔH_{sub} for the ruthenium-pentaammine complexes was proportional to the spectroscopically estimated stabilization energy [45]. Thus, ΔH_{sub} can be used as a qualitative measure of the π-electron acceptability of L, but such values for the complexes in this study are rarely available. Pickett and Pletcher [46] defined the ligand constant, P_L, which stands for the contribution of L to the redox potential of the complexes, as in Eq. (3).

$$P_L = E_{1/2}\{[Cr(CO)_5(L)]\} - E_{1/2}\{[Cr(CO)_6]\} \quad (3)$$

A ligand constant like P_L can be used instead of ΔH_{sub}. This ligand constant is a more favorable measure for the π-electron acceptability of L, because it is readily determined under the same conditions as those in this study. Accordingly, such a ligand constant was defined for ruthenium-pentaammine complexes as in Eq. (4).

$$P_L(Ru) = E_{1/2}\{[Ru(NH_3)_5(L)]\} - E_{1/2}\{[Ru(NH_3)_5(H_2O)]\} \quad (4)$$

Fig. 12 shows the plot of P_L(Ru) against ΔH_{sub} for $[Ru(NH_3)_5(L)]^{2+}$ (L: N_2, DMSO, pz, isn, py, and

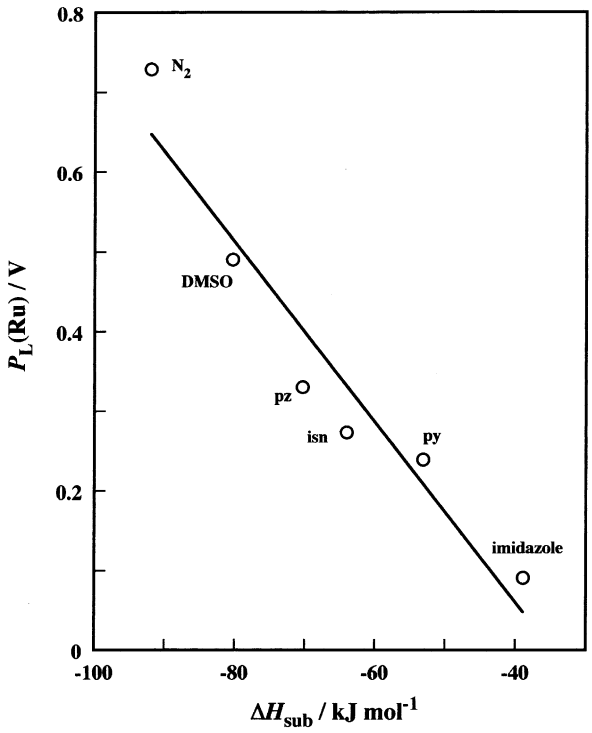

Fig. 12. Plot of P_L(Ru) against ΔH_{sub} for $[Ru(NH_3)_5(L)]^{2+}$ (L: N_2, DMSO, pz, isn, py, and imidazol).

imidazole). The values of P_L(Ru) were calculated by Eq. (4), using $E_{1/2}$ in water for the pentaammine complexes. These $E_{1/2}$ values were estimated by

$$E_{1/2}(\text{calcd}) = 1.14 \sum E_L - 0.35 \quad (5)$$

using the ligand parameters, E_L, proposed by Lever [47]. The linear relationship reveals that P_L(Ru) can be used as a measure of the π-electron acceptability of L; a ligand with a large P_L(Ru) value has a large acceptability for π-electrons.

In order to investigate the effect of the π-electron acceptability of L upon $\Delta E_{1/2}$(lim) caused by adduct formation with 18C6, $\Delta E_{1/2}$(lim) was plotted against P_L(Ru). The values of P_L(Ru) were calculated using $E_{1/2}$ for the complexes in Table 7. $[Ru(NH_3)_5(CH_3CN)](PF_6)_2$ ($E_{1/2}$ = 0.173 V versus ($AgNO_3$/Ag)) was used as a standard complex in the calculation of P_L(Ru) instead of $[Ru(NH_3)_5(H_2O)](PF_6)_2$, because the aqua ligand in $[Ru(NH_3)_5(H_2O)](PF_6)_2$ is gradually substituted by acetonitrile as the solvent. The plot for pentaammine–ruthenium complexes in Fig. 13 shows that the absolute value of $\Delta E_{1/2}$(lim) decreases with increasing P_L(Ru) in a linear manner; that is, the net change in redox potential caused by the adduct formation is smaller for the complex involving L with greater π-electron acceptability. This interpretation was supported by stability constants of the crown ether adducts described in Section 4.

On the other hand, in order to examine the influence from the crown ether itself, the electrochemical behavior of a representative ruthenium–ammine complex $[Ru(NH_3)_5(py)](PF_6)_2$ was investigated by cyclic voltammetry in the absence and presence of various crown ethers. The $\Delta E_{1/2}$(lim) values were obtained from the dependence of $\Delta E_{1/2}$ on the crown ether concentration, as mentioned above, and are summarized in Table 8. The absolute values of $\Delta E_{1/2}$(lim) increase with the size of the crown ether ring in each series of crown ethers: 12C4 to18C6, DC18C6 to DC24C8, and DB18C6 to DB30C10. For a series of crown ethers with the same ring size, $|\Delta E_{1/2}(\text{lim})|$ decreases in the order 18C6 > DC18C6 ≈ B18C6 > DB18C6 and DC24C8 > DB24C8. When a cyclohexano and a phenyl ring are introduced into the crown ether, the values of $|\Delta E_{1/2}(\text{lim})|$ decrease. A large decrease in $|\Delta E_{1/2}(\text{lim})|$

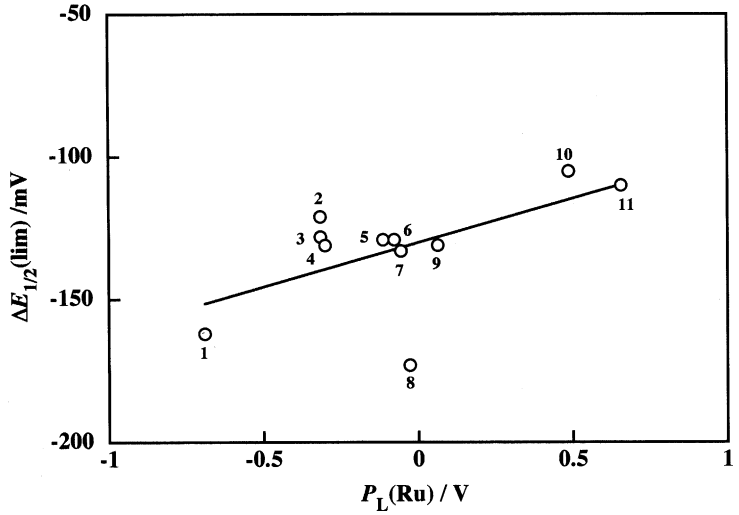

Fig. 13. Plot of $\Delta E_{1/2}$(lim) against P_L(Ru) for pentaammineruthenium complexes: (1) $[Ru(NH_3)_5(Cl)](PF_6)_2$, (2) $[Ru(NH_3)_5(dmapy)](PF_6)_3$, (3) $[Ru(NH_3)_5(MeIm)](PF_6)_3$, (4) $[Ru(NH_3)_5(ampy)](PF_6)_3$, (5) $[Ru(NH_3)_5(py)](PF_6)_2$, (6) $[Ru(NH_3)_5(4,4'\text{-bpy})](PF_6)_2$, (7) $[Ru(NH_3)_5(isn)](PF_6)_2$, (8) $[Ru(NH_3)_5(dmabn)](PF_6)_2$, (9) $[Ru(NH_3)_5(pz)](PF_6)_2$, (10) $[Ru(NH_3)_5(Mepz)](PF_6)_3$, (11) $[Ru(NH_3)_5(N_2)](PF_6)_2$. Datum for $[Ru(NH_3)_5(N_2)](PF_6)_2$ is change in peak potential of its oxidation on addition of 0.10 mol dm^{-3} 18C6 to the complex solution of 5.0×10^{-4} mol dm^{-3} in acetonitrile.

Table 8
Limiting values of change in redox potential, $\Delta E_{1/2}$(lim), for the Ru(III)–Ru(II) redox couple in $[Ru(NH_3)_5(py)](PF_6)_2$ caused by addition of crown ether in acetonitrile

Crown ether	$\Delta E_{1/2}$(lim) (mV)	
12C4	>−30[a]	
15C5	−130 (4)[a]	
18C6	−129 (2)[a]	
B18C6	−92 (2)[a]	
DC18C6	−87 (2)[a]	
DC24C8	−115 (3)[a]	
DB18C6[b]	−15[c]	−6 (2)[d]
DB24C8[b]	−29 (2)[a]	−12 (2)[d]
DB30C10[b]	−143[c]	−59 (3)[d]

The values in parentheses are the standard deviations.
[a] [complex] = 5.0×10^{-4} mol dm^{-3}.
[b] The values were $\Delta E_{1/2}$ on addition of 200-fold excess of crown ether.
[c] These values are normalized by use of the ratio of both $\Delta E_{1/2}$ values for the DB24C8 system under the conditions of footnotes 'a' and 'd'.
[d] [complex] = 1.0×10^{-4} mol dm^{-3}.

was brought about by the introduction of the more rigid phenyl ring. The ring size and the introduction of a cyclohexano and a phenyl ring affect the flexibility of crown ether rings and hence causes the variation in $|\Delta E_{1/2}(\text{lim})|$. A more flexible crown ether gives a greater $|\Delta E_{1/2}(\text{lim})|$ on forming adducts, presumably because more flexible crown ethers are able to adopt a more favorable configuration for hydrogen bonding with the ammines coordinating to ruthenium.

Thus, hydrogen bonding brings about a prominent change in redox potential of the complex and the change in redox potential is affected by the following factors: (i) the number of ammine ligands coordinating to ruthenium, (ii) the π-electron acceptability of a ligand not interacting with crown ethers, and (iii) the flexibility of the crown ether ring.

4. Stability constants of crown ether adducts

Stability constants offer much information about the adduct formation of ruthenium–ammine complexes and are necessary to understand the electrochemical behavior of those complexes on addition of crown ethers as mentioned in the previous section. Some attempts were performed to evaluate the stability constants of the 18C6 adduct.

In principle, the stability constant can be evaluated from the results of the Job's continuous variation method mentioned in Section 2. However, it is hard to obtain a reliable value because of the small change in absorbance caused by adduct formation. Partition chromatography is applicable to determine the stability constants of the 18C6 adducts. For the ruthenium(II)–ammine complexes with ligands having only pyridine moieties as ancillary ligands, the stability constants were obtained by Miyajima's method [48,49]

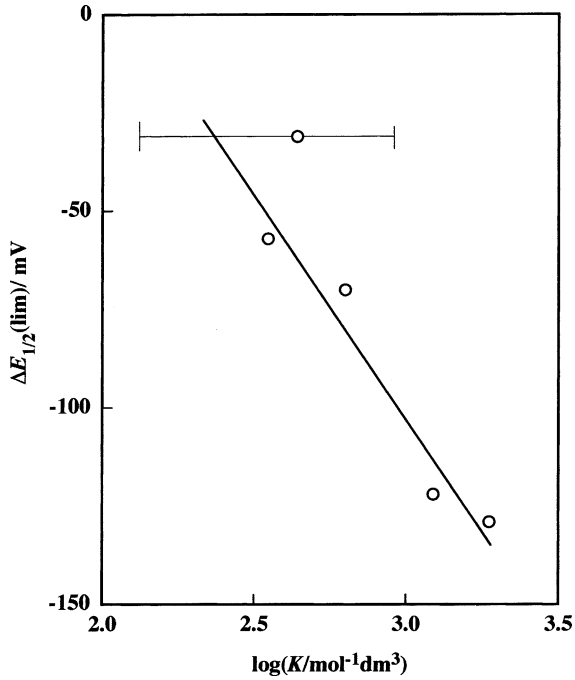

Fig. 14. Relation between $\Delta E_{1/2}$(lim) and log K for $[Ru(NH_3)_n(L)(L')](PF_6)_2$ (n = 1–5; L, L′: py, bpy, and/or trpy).

using HPLC. The stability constants were obtained from dependences of the capacity factor of the complex on 18C6 concentrations. The correlation between the stability constants $(K_{II})_1$, and $\Delta E_{1/2}$(lim) was examined as shown in Fig. 14. The plot shows a linear correlation and implies that $\Delta E_{1/2}$(lim) reflects the stability of the adduct as to the ruthenium–ammine complexes which involve pyridine moieties as ancillary ligands. Unfortunately, this technique has a very restricted application, because of the strong adsorption of complexes to the packing materials.

Although the true stability constant of the adduct cannot be obtained from the dependences of the change in the redox potential on crown ether concentrations (Fig. 10), a relative stability constant can be estimated.

Equilibria of adduct formation with crown ethers (C) are expressed for a rutheniun(II) complex and a ruthenium(III) complex on the basis of the stoichiometries of adduct formation as follows (Eqs. (6)–(8)).

$$\text{Ru(II)} + \text{C} \rightleftharpoons \text{Ru(II)} \cdot \text{C}; \qquad (K_{II})_1 = \frac{[\text{Ru(II)} \cdot \text{C}]}{[\text{Ru(II)}][\text{C}]} \tag{6}$$

$$\text{Ru(III)} + \text{C} \rightleftharpoons \text{Ru(III)} \cdot \text{C}; \qquad (K_{III})_1 = \frac{[\text{Ru(III)} \cdot \text{C}]}{[\text{Ru(III)}][\text{C}]} \tag{7}$$

$$\text{Ru(III)} \cdot \text{C} + \text{C} \rightleftharpoons \text{Ru(III)} \cdot \text{C}_2; \quad (K_{III})_2 = \frac{[\text{Ru(III)} \cdot \text{C}_2]}{[\text{Ru(III)} \cdot \text{C}][\text{C}]} \tag{8}$$

Table 9
Stability constants for adducts of $[Ru(NH_3)_5(py)](PF_6)_2$ with crown ethers in acetonitrile

Crown ether	$(K_{II})_1$ (10^2 mol^{-1} dm^3)	$(K_{III})_1$ (10^2 mol^{-1} dm^3)	$(K_{III})_2$ (10^2 mol^{-1} dm^3)
12C4	–	–	–
15C5	0.14 ± 0.09	2.0 ± 0.89	1.6 ± 0.93
18C6	1.6 ± 1.4	9.1 ± 2.4	3.5 ± 3.0
B18C6	0.32 ± 0.24	2.5 ± 0.13	0.49 ± 0.34
DC18C6	0.21 ± 0.33	5.0 ± 0.88	0.12 ± 0.22
DC24C8	0.50 ± 0.78	3.9 ± 0.49	0.74 ± 1.1

The change in the redox potential of the metal center of the ruthenium–ammine complex is expressed as Eq. (9).

$$\Delta E_{1/2} = 59\,(\mathrm{mV}) \log \frac{1 + (K_{II})_1[C]}{1 + (K_{III})_1 \cdot [C] + (K_{III})_1 \cdot (K_{III})_2[C]^2} \quad (9)$$

Accordingly, stability constants of adducts can be evaluated from the dependence of $\Delta E_{1/2}$ on crown ether concentrations by least squares analysis of Eq. (9), which was carried out with the data in Table 8 for $[Ru(NH_3)_5(py)](PF_6)_2$. The stability constants obtained are listed in Table 9. The values of $(K_{II})_1$ roughly parallel the values of $\Delta E_{1/2}$(lim) in Table 8. The value of $(K_{II})_1$ in the 18C6 system is much greater than that in the 15C5 system though both systems exhibited similar $\Delta E_{1/2}$(lim). This implies that 18C6 adopts a more suitable configuration for hydrogen bonding with the ammine ligands. The values of $(K_{III})_1$ are larger than those of $(K_{II})_1$ in all crown ether systems and this tendency indicates that the ruthenium(III)–ammine complex forms a more stable adduct than the ruthenium(II)–ammine complex does, in agreement with the acidity of the ammine ligands in their complexes.

trans-Ammine proton NMR signals were observed for $[Ru(NH_3)_5(pz)](PF_6)_2$ and $[Ru(NH_3)_5(Mepz)](PF_6)_3$ at various 18C6 concentrations. The results are shown in Fig. 15 [50]. The *trans*-ammine proton signals shifted continuously toward a lower magnetic field with increasing 18C6 concentration for both complexes. Using Eq. (5), the observed chemical shifts in the presence of 18C6 are apparent values, δ_{app}, and can be expressed as follows.

$$\delta_{app} = \frac{\delta_{ML}[Ru(II)] + \delta_{add}[Ru(II) \cdot C]}{[Ru(II)]_T},$$
$$[Ru(II)]_T = [Ru(II)] + [Ru(II) \cdot C] \quad (10)$$

where δ_{ML}, δ_{aadd}, and $[Ru(II)]_T$ denote the chemical shifts of the ruthenium(II) complex and their 18C6 adduct, and the total concentration of the ruthenium(II) complex, respectively. The above expression can be replaced using the stability constant of the 18C6 adduct as Eq. (11):

$$\delta_{app} = \frac{\delta_{ML} - \delta_{add}}{(K_{II})_1[C] + 1} + \delta_{add} \quad (11)$$

The diffusion coefficient also decreased continuously with increasing 18C6 concentration, as shown in Fig. 16. Ac-

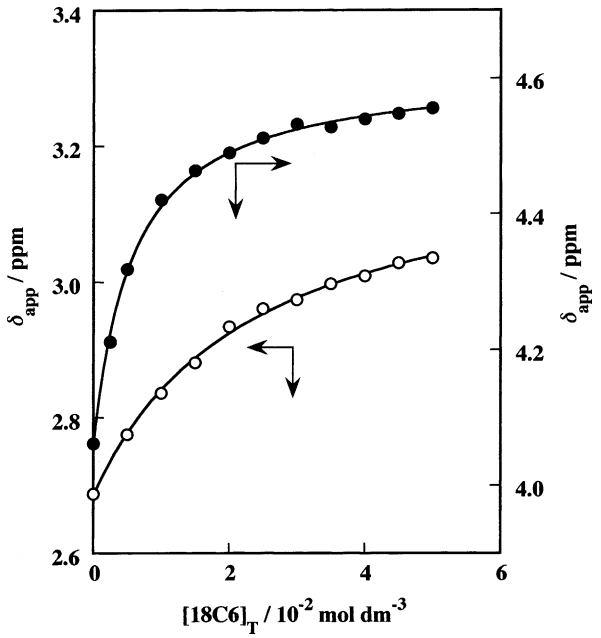

Fig. 15. Dependences of the chemical shift of *trans*-ammine protons for $[Ru(NH_3)_5(pz)](PF_6)_2$ (open circles) and $[Ru(NH_3)_5(Mepz)](PF_6)_3$ (filled circles) on 18C6 concentration. Solid lines represent the regression lines of Eq. (2) ([complex] = 5.0×10^{-4} mol dm^{-3}).

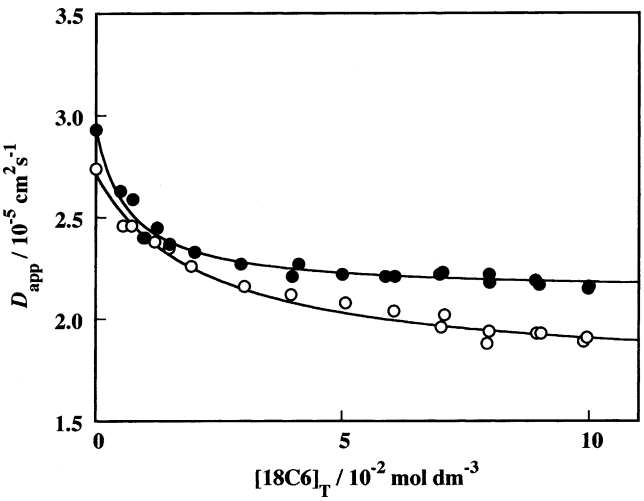

Fig. 16. Dependences of apparent diffusion coefficients for $[Ru(NH_3)_5(pz)](PF_6)_2$ (open circles) and $[Ru(NH_3)_5(Mepz)](PF_6)_3$ (filled circles) on the 18C6 concentration. Solid lines represent the regression lines of Eq. (3) ([complex] = 5.0×10^{-4} mol dm^{-3}).

Table 10
Stability constants, $(K_{II})_1$, for the 18C6 adducts for ruthenium(II) complex[a]

	$[Ru(NH_3)_5(pz)](PF_6)_2$	$[Ru(NH_3)_5(pzMe)](PF_6)_3$
Voltammetry	3.1 ± 33	$(8.9 \pm 2.8) \times 10$
^{1}H NMR	$(4.26 \pm 0.35) \times 10$	$(1.75 \pm 0.10) \times 10^2$
Chronocoulometry	$(4.51 \pm 0.49) \times 10$	$(1.49 \pm 0.17) \times 10^2$

[a] Unit of stability constant is $mol^{-1}\,dm^3$.

cordingly, the apparent diffusion coefficient, D_{app}, can be expressed by Eq. (12).

$$D_{app} = \frac{D_{ML} - D_{add}}{(K_{II})_1[C] + 1} + D_{add} \quad (12)$$

where D_{ML} and D_{add} denote the diffusion coefficients of the ruthenium(II) complex and its 18C6 adduct, respectively.

Stability constants of 18C6 adducts were obtained for $[Ru(NH_3)_5(pz)](PF_6)_2$ and $[Ru(NH_3)_5(Mepz)](PF_6)_3$ by the least squares analysis of Eqs. (11) and (12) with the data in Figs. 15 and 16, and are listed in Table 10. Table 10 also lists the stability constants obtained from the dependences of the change in redox potential of metal-centered oxidation on the 18C6 concentration. The stability constants are in good agreement with each other and with those determined by methods other than voltammetry, although the ones estimated by voltammetry show smaller values than others for the reason mentioned above. It is clear that the true stability constants of a 18C6 adduct can be evaluated by ^{1}H NMR spectroscopy and chronocoulometry. The difference between the stability constants of 18C6 adducts for $[Ru(NH_3)_5(pz)](PF_6)_2$ and $[Ru(NH_3)_5(Mepz)](PF_6)_3$ supports the idea, that the π-electron acceptability of ancillary ligands is the principal difference in the properties of both complexes.

5. Adduct formation of mixed-valence binuclear complex

The second-sphere coordination of crown ethers should influence the electron transfer properties of ammine complexes. Adduct formation of mixed-valence binuclear complexes is interesting because they are important species as an intermediate in electron transfer between metal complexes [51–63]. For a mixed-valence binuclear ammine-complex with localized valence as depicted on top of Scheme 4, Hupp and co-workers reported the second-sphere coordination of dibenzo-24-crown-8 ether to $[(NH_3)_5Ru(II)(4,4'\text{-bpy})\text{-}Ru(III)(NH_3)_5]^{5+}$ (4,4′-bpy: 4,4′-bipyridine) [53]. This complex showed the Ru(II) to 4,4′-bpy charge-transfer (MLCT) band in the visible region and the intervalence transfer between Ru(II) and Ru(III) (IT) band in the near-infrared region. The energy of the MLCT band decreased monotonously with increasing concentration of crown ether. However, the energy of the IT band showed an initial sharp rise and then

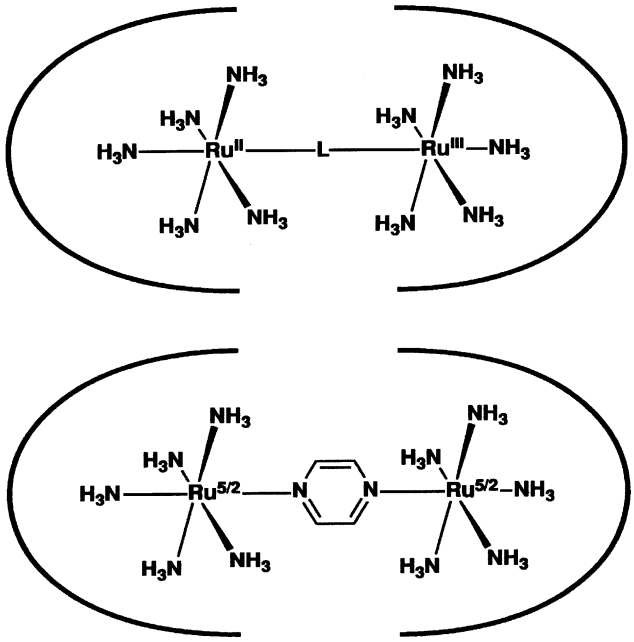

Scheme 4. Schematic representations for mixed-valence binuclear complexes.

gradual decrease with increasing concentration of crown ether. They interpreted the dependence of the intervalence absorption energy as the asymmetric binding of crown ether first at $Ru(III)(NH_3)_5$ and then symmetrical binding at $Ru(II)(NH_3)_5$. The second-sphere coordination of 18C6 to the mixed-valence complex with localized valence is easily predicted based on the results of mononuclear ruthenium(II)– and ruthenium(III)–pentaammine complexes in Section 2: one molecule of 18C6 interacts at ruthenium(II) end and two molecules of 18C6 bind at the ruthenium(III) end.

The Creutz–Taube ion, $[(NH_3)_5Ru^{5/2}(pz)Ru^{5/2}(NH_3)_5]^{5+}$, is a typical class III mixed-valence binuclear complex. In class III mixed-valence complexes depicted on the bottom of Scheme 4, the valences of the metal centers are delocalized and there are no discrete Ru(II) and Ru(III) centers, but formally only two Ru(2.5) centers [64–67]. It would be interesting to learn how the crown ether interacts with the Creutz–Taube ion. The Creutz–Taube ion exhibits a charge-transfer (usually described as metal-to pyrazine charge transfer) band in the visible region and the IT band in the near-infrared region. Hupp et al. reported encapsulation of the Creutz–Taube ion with dibenzo-crown ethers with a ring size of 24–42 in nitromethane [68,69] The IT band of Creutz–Taube ion showed characteristics of delocalized system; narrow bandwidth, low energy, asymmetric line shape, and high intensity. In the presence of one equivalent of the crown ether, the IT band shifted to higher energy with broadening and loss of peak intensity. By adding a large amount of crown ether, the initial spectrum was essentially recovered. The IT band behavior is similar to that of $[(NH_3)_5Ru(II)(4,4'\text{-bpy})Ru(III)(NH_3)_5]^{5+}$. A plot of

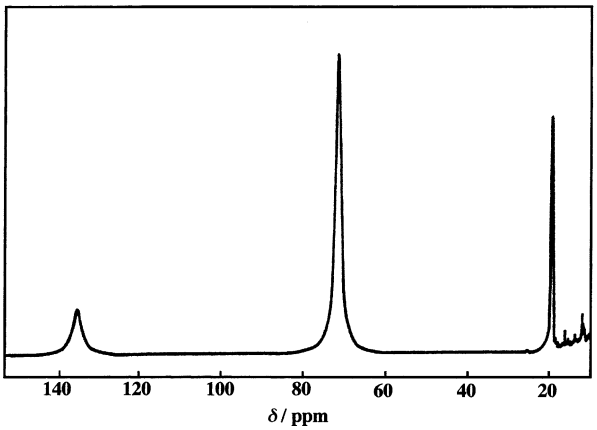

Fig. 17. ^{1}H NMR spectrum of $[(NH_3)_5Ru(pz)Ru(NH_3)_5](PF_6)_5$ in deuterated acetone ([complex] $= 1.0 \times 10^{-2}$ mol dm^{-3}).

bandwidth of IT band versus crown: complex ratio showed a maximum at 1:1 stoichiometry. This was interpreted as the first asymmetric binding and then the second symmetric binding of crown ether. The asymmetric binding of a single crown ether induces localization (or partial localization) and the symmetric binding of a second crown ether restores delocalization. The charge-transfer band in the visible region also shifted to lower energy opposite to the IT band shift. Its extent was dependent on the ring size of the crown ether and larger than those of IT band on binding of a second crown ether. Electrochemical measurements gave a negative shift in the formal potential of two redox couples, Ru–Ru$^{(5+/4+)}$ and Ru–Ru$^{(6+/5+)}$: $\Delta E^{(5+/4+)}$ was larger than $\Delta E^{(6+/5+)}$.

For the 18C6 system, the CT band in the visible region of the Creutz–Taube ion shifted to longer wavelength with increasing 18C6 concentration in a manner similar to the corresponding mononuclear pyrazine complex. (see Section 2) However, the shift of the IT band was obscured on addition of 1000-fold excess of 18C6 owing to insensitivity to 18C6 binding.

The second-sphere coordination of 18C6 to the Creutz–Taube ion was also investigated by ^{1}H NMR spectroscopy [35]. Fig. 17 shows ^{1}H NMR spectrum of the Creutz–Taube ion in deuterated acetone. Broad signals were observed at 19, 71, and 133 ppm, and were assigned to the ring protons of coordinated pyrazine and the *cis*- and *trans*-ammine protons, respectively, according to the literature [70,71]. Fig. 18 shows the dependencies of the chemical shifts of those signals on 18C6 concentration. The *trans*-ammine proton signal initially shifted to a lower magnetic field with increasing 18C6 concentration and showed the shift to lowest magnetic field at a concentration of 3×10^{-2} mol dm^{-3} 18C6. In the concentration range of 18C6 more than 3×10^{-2} mol dm^{-3}, the *trans*-ammine proton signal began to go back to the chemical shift of the *trans*-ammine proton of the complex itself, accompanied by a downfield-shift of the *cis*-ammine proton signal. This change indicates that 18C6 initially binds to the Creutz–Taube ion at the *trans*-ammine and the binding at the *trans*-ammine is gradually replaced by binding

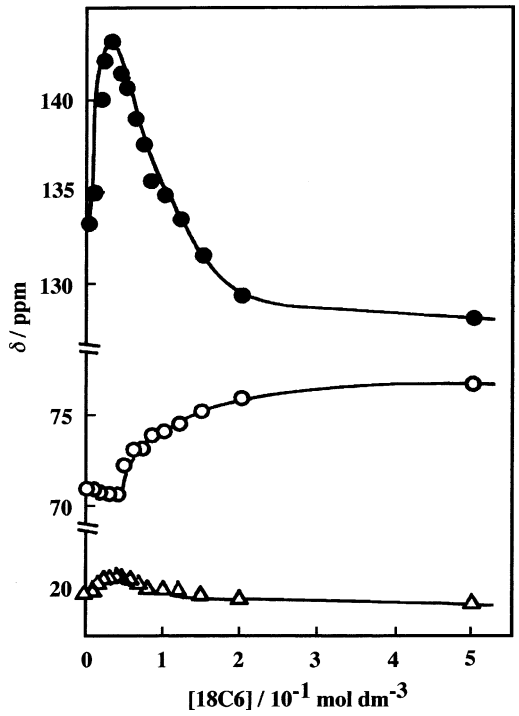

Fig. 18. Dependence of the chemical shifts of the pyrazine protons (△) and the *cis*-ammine (○) and *trans*-ammine protons (●) of $[(NH_3)_5Ru(pz)Ru(NH_3)_5](PF_6)_5$ on 18C6 concentration ([complex] $= 1.0 \times 10^{-2}$ mol dm^{-3}).

at the *cis*-ammine with increasing 18C6 concentration. In other words, 18C6 successively forms adducts having the complex-to-18C6 stoichiometry of 1:1, 1:2, 1:3, and 1:4 with increasing 18C6 concentration, as schematically depicted in Scheme 5. The behavior of the *trans*-ammine proton signal corresponds with that of bandwidth of the IT band at half height for the Creutz–Taube ion on addition of dibenzo-crown ethers observed by Hupp and co-workers [69]. For the 18C6 system, the formation of an asymmetric 1:3 adduct is strongly supported by the isolation of 18C6 adduct of the Creutz–Taube ion described in Section 2. The formation of the asymmetric 18C6 adduct may induce localization of delocalized valence in Creutz–Taube ion as reported by Hupp, since it is predicted from the results of mononuclear ruthenium pentaammine complexes that the mixed-valence binuclear rutheniumammine complex can form an asymmetric adduct binding one molecule of 18C6 at Ru(II) end and two molecules of 18C6 at Ru(III) end. The electrochemical properties of the Creutz–Taube ion are also affected by 18C6 binding. Fig. 19 shows the cyclicvoltammograms of the Creutz–Taube ion in acetonitrile in the absence and presence of 18C6. Two reversible redox couples were observed at 0.138 and 0.57 V versus ($AgNO_3$/Ag) and correspond to Ru–Ru$^{(5+/4+)}$ and Ru–Ru$^{(6+/5+)}$ redox processes, respectively [45]. On addition of 18C6, two redox couples shifted continuously toward negative potential with increasing 18C6 concentration, maintaining their reversibility. The degree in those shifts is larger for Ru–Ru$^{(5+/4+)}$

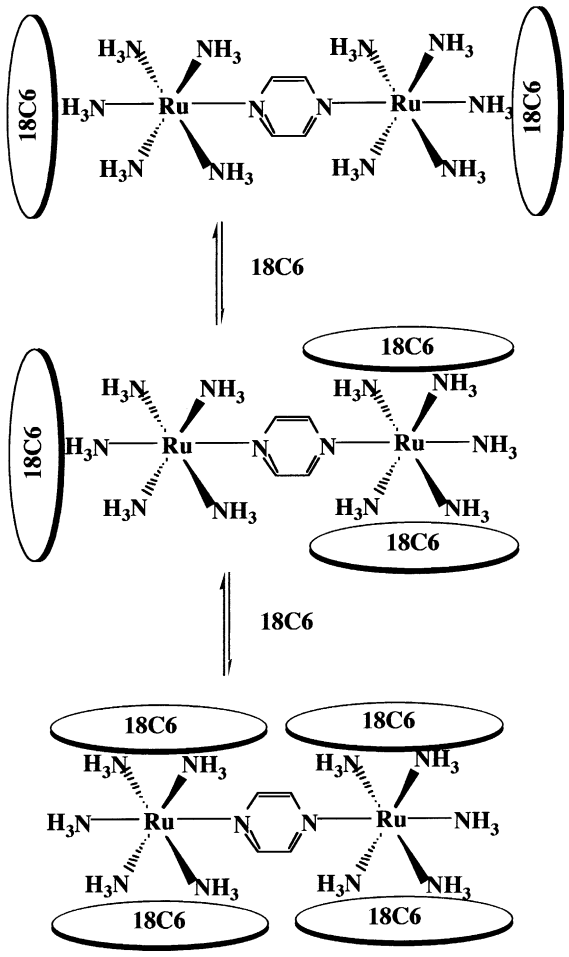

Scheme 5. Schematic representation for stepwise adduct formation of the mixed-valence binuclear complex.

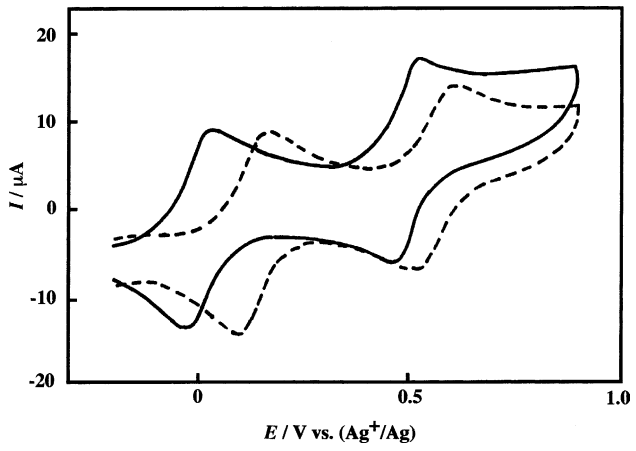

Fig. 19. Cyclic voltammograms of 5.0×10^{-4} mol dm^{-3} $[(NH_3)_5Ru(pz)Ru(NH_3)_5](PF_6)_5$ in 0.1 mol dm^{-3} tetrabutylammonium hexafluorophosphate acetonitrile solution in the absence (- - -) and presence (—) of 0.1 mol dm^{-3} 18C6.

than for Ru–Ru$^{(6+/5+)}$ and the difference increased with increasing 18C6 concentration. This implies that 18C6 binding stabilizes the higher oxidation state more than lower one and the extent in stabilization is different between redox processes.

6. Conclusions

We have demonstrated that ruthenium–ammine complexes interact with 18C6 in the second sphere and form adducts through hydrogen bonding between the coordinating ammines to ruthenium and the ether oxygen atoms of 18C6. The active sites and the stoichiometry of adduct formation are dependent on the valence of the metal center: the ruthenium(II) complex forms an 1:1 adduct with 18C6, interacting with the *trans*-ammine of the complex, while the ruthenium(III) complex forms a 1:2 adduct, with 18C6 interacting with the *cis*-ammines of the complex. This hydrogen bonding exhibits a significant change in the redox potential of the complex, which is affected by the following factors: (i) the number of ammine ligands coordinating to ruthenium, (ii) the π-electron acceptability of a ligand not interacting with crown ethers, and (iii) the flexibility of the crown ether ring. Combinations of those factors make it possible to design a supramolecular species with a desired range of redox potentials. Furthermore, the binuclear complex with a delocalized mixed-valence state forms an asymmetric 1:3 adduct with 18C6, having 1:1 stoichiometry at one pentaammine moiety and 1:2 stoichiometry at the other moiety, implying a valence-trap.

We conclude that micro-environmental changes around the metal complex induced by second-sphere coordination such as hydrogen bonding can provide a device to tune the redox potential of the metal complexes.

References

[1] J.-M. Lehn, Angew. Chem., Int. Ed. Engl. 27 (1988) 89.
[2] H.M. Colquhoun, J.F. Stoddart, D.J. Williams, Angew. Chem., Int. Ed. Engl. 25 (1986) 487.
[3] V. Balzani, N. Sabbatini, F. Scandola, Chem. Rev. 86 (1986) 319.
[4] A. Werner, Ann. Chem. 386 (1912) 1.
[5] J.C. Curtis, B.P. Sullivan, T.J. Meyer, Inorg. Chem. 22 (1983) 224.
[6] C. Creutz, M.H. Chou, Inorg. Chem. 26 (1987) 2995.
[7] R.S. Drago, D.E. Richardson, J.E. George, Inorg. Chem. 36 (1997) 25.
[8] V. Gutmann, The Donor–Acceptor Approachh to Molecular Interaction, Plenum Press, New York, 1980.
[9] P.G. Eller, R.A. Penneman, Inorg. Chem. 15 (1976) 2439.
[10] T.B. Vance Jr., E.M. Holt, C.G. Pierpont, S.M. Holt, Acta Cryst. B36 (1980) 150.
[11] T.B. Vance Jr., E.M. Holt, D.L. Varie, S.M. Holt, Acta Cryst. B36 (1980) 153.
[12] F.M. Raymo, J.F. Stoddart, Chem. Ber. 129 (1996) 981.
[13] B. Ji, Z. Zhou, K. Ding, Y. Li, Polyhedron 17 (1998) 4327.
[14] R.S. Shanmugasundara, H.-K. Fun, Polyhedron 20 (2001) 2145.

[15] H.M. Colquhoun, S.M. Doughty, J.F. Stoddart, D.J. Williams, Angew. Chem., Int. Ed. Engl. 23 (1984) 235.
[16] P.C. Junk, L.M. Louis, M.K. Smith, Z. Anorg. Allg. Chem. 628 (2002) 1196.
[17] D. Reinen, M. Atanasov, S.-L. Lee, Coord. Chem. Rev. 175 (1998) 91.
[18] A.M. Zwickel, C. Creutz, Inorg. Chem. 10 (1971) 2395.
[19] G.M. Bryant, J.E. Fergusson, H.K.J. Powell, Aust. J. Chem. 24 (1971) 257.
[20] D.K. Lavallee, E.B. Fleisher, J. Am. Chem. Soc. 94 (1972) 2583.
[21] J.E. Sutton, H. Taube, Inorg. Chem. 20 (1981) 4021.
[22] R.S. da Silra, S.I. Gorelsky, E.S. Dodsworth, E. Tfouni, A.B.P. Lever, J. Chem. Soc., Dalton Trans., 4078 (2000).
[23] C.R. Johnson, W.W. Henderson, R.E. Shepherd, Inorg. Chem. 23 (1984) 27564.
[24] J.R. Winkler, T.L. Netzel, C. Creutz, N. Sutin, J. Am. Chem. Soc. 109 (1987) 2381.
[25] I. Ando, H. Fujimoto, K. Nakayama, K. Ujimoto, H. Kurihara, Polyhedron 10 (1991) 1139.
[26] I. Ando, D. Ishimura, M. Mitsumi, K. Ujimoto, H. Kurihara, Polyhedron 11 (1992) 2335.
[27] I. Ando, T. Tsuji, K. Ujimoto, H. Kurihara, Fukuoka Univ. Sci. Rep. 25 (1995) 119.
[28] I. Ando, D. Ishimura, K. Ujimoto, H. Kurihara, Inorg. Chem. 35 (1996) 3504.
[29] I. Ando, D. Ishimura, M. Mitsumi, K. Ujimoto, H. Kurihara, Inorg. Chim. Acta 249 (1996) 201.
[30] H.M. Colquhoun, J.F. Stoddart, D.J. Williams, J.B. Wolstenholme, R. Zarzycki, Angew. Chem., Int. Ed. Engl. 20 (1981) 1051.
[31] X.-J. Yang, B. Wu, W.-H. Sun, C. Janiak, Inorg. Chim. Acta 343 (2003) 366.
[32] S. Dhungana, P.S. White, A.L. Crumbliss, J. Am. Chem. Soc. 125 (2003) 14760.
[33] D.R. Alston, A.M.Z. Slawin, J.F. Stoddart, R. Zarzycki, Angew. Chem., Int. Ed. Engl. 26 (1987) 693.
[34] M. Todd, Y. Dong, J. Honey, J.T. Hupp, Inorg. Chem. 32 (1993) 2001.
[35] I. Ando, D. Ishimura, K. Ujimoto, H. Kurihara, Inorg. Chem. 33 (1994) 5010.
[36] R.G. Gaunder, H. Taube, Inorg. Chem. 9 (1970) 2627.
[37] J.E. Sutton, H. Taube, Inrog. Chem. 20 (1981) 3125.
[38] D.I. Yoon, S. Belanger, J.T. Hupp, C.L. Stern, Acta Cryst. C54 (1998) 1427.
[39] I. Ando, M. Higashi, K. Ujimoto, H. Kurihara, Inorg. Chim. Acta 282 (1998) 247.
[40] K.G. Pachler, F. Matlok, H.-U. Grenlich, Merk FT-IR Atlas, VCH, Weinheim, 1988, p. 882.
[41] H.S. Lin, D.J. Barclay, F.C. Anson, Inorg. Chem. 11 (1972) 1460.
[42] T. Matsubara, P.C. Ford, Inorg. Chem. 15 (1976) 1107.
[43] C.A. Stein, H. Taube, J. Am. Chem. Soc. 100 (1978) 1635.
[44] K.M. Davies, B. Guilani, Inorg. Chim. Acta 127 (1987) 223.
[45] J.F. Wishart, H. Taube, K.J. Breslauer, S.S. Isied, Inorg. Chem. 23 (1984) 2997.
[46] C.J. Pickett, D.J. Pletcher, J. Organomet. Chem. 102 (1975) 327.
[47] A.B.P. Lever, Inorg. Chem. 29 (1990) 1271.
[48] T. Miyajima, N. Yoza, S. Ohashi, Anal. Lett. 10 (1977) 709.
[49] T. Miyajima, M. Ibaragi, N. Yoza, S. Ohashi, J. Liq. Chromatogr. 4 (1981) 259.
[50] I. Ando, K. Nishihara, K. Ujimoto, H. Kurihara, Inorg. Chim. Acta 346 (2003) 19.
[51] C. Creutz, Prog. Inorg. Chem. 30 (1983) 1.
[52] A. Haim, Prog. Inorg. Chem. 30 (1983) 273.
[53] M.D. Todd, Y. Dong, J.T. Hupp, Inorg. Chem. 30 (1991) 4685.
[54] F.W. Vance, L. Karki, J.K. Reigle, J.T. Hupp, J. Phys. Chem. 102 (1998) 8320.
[55] I. de S. Moreira, D.W. Franco, J. Chem. Soc., Chem. Commun. 450 (1992).
[56] A.-C. Ribou, J.-P. Launay, K. Takahashi, T. Nihira, S. Tarutani, C.W. Spangler, Inorg. Chem. 33 (1994) 1325.
[57] A.E. Almaraz, L.A. Gentil, L.M. Baraldo, J.A. Olabe, Inorg. Chem. 35 (1996) 7718.
[58] S.K. Dutta, J. Ensling, R. Werner, U. Florke, W. Haase, P. Gutlich, K. Nag, Angew. Chem., Int. Ed. Engl. 36 (1997) 152.
[59] C. Wang, B.K. Mohney, R.D. Williams, V. Petrov, J.T. Hupp, G.C. Walker, J. Am. Chem. Soc. 120 (1998) 5848.
[60] M.D. Shores, J.R. Long, J. Am. Chem. Soc. 124 (2002) 3512.
[61] R.C. Rocha, H.E. Toma, Polyhedron 21 (2002) 2089.
[62] K.M. Kadish, L.-L. Wang, A. Thuriere, E. van Caemelbeke, J.L. Bear, Inorg. Chem. 42 (2003) 834.
[63] M.E.G. Posse, M.M. Vergara, F. Fagalde, N.E. Katz, Poyhedron 22 (2003) 465.
[64] C. Creutz, H. Taube, J. Am. Chem. Soc. 91 (1969) 3988.
[65] U. Furholtz, H. Bugi, F. Wagner, A. Stebler, J. Ammeter, E.R. Kraus, R.J.H. Clark, M.J. Stead, A. Ludi, J. Am. Chem. Soc. 106 (1984) 121.
[66] S.P. Best, R.J.H. Clark, R.C.S. McQueen, S. Joss, J. Am. Chem. Soc. 111 (1989) 548.
[67] S.B. Piepho, J. Am. Chem. Soc. 112 (1990) 4197.
[68] J.T. Hupp, Y. Dong, Inorg. Chem. 33 (1994) 4421.
[69] Y. Dong, J.T. Hupp, D.I. Yoon, J. Am. Chem. Soc. 115 (1993) 4379.
[70] J.H. Eliesand, R.S. Drago, Inorg. Chem. 11 (1972) 415.
[71] B.C. Buncer, R.S. Drago, D.N. Hendrickson, R.M. Richman, S.L. Kessell, J. Am. Chem. Soc. 100 (1978) 3805.